THE ASTRONOMICAL JOURNAL, 115:1295–1318, 1998 April

SUB-MILLIARCSECOND IMAGING OF QUASARS AND ACTIVE GALACTIC NUCLEI

K. I. KELLERMANN
National Radio Astronomy Observatory,[1] 520 Edgemont Road, Charlottesville, VA 22903; kkellerm@nrao.edu
R. C. VERMEULEN
Netherlands Foundation for Research in Astronomy, Postbus 2, NL-7990 AA Dwingeloo, Netherlands; rcv@nfra.nl
J. A. ZENSUS
Max-Planck-Institut für Radioastronomie, Auf dem Hugel 69, D-53121 Bonn, Germany; azensus@mpifr-bonn.mpg.de
AND
M. H. COHEN
Department of Astronomy, Mail Stop 105-24, California Institute of Technology, Pasadena, CA 91125; mhc@astro.caltech.edu
Received 1997 November 17; revised 1997 December 22

ABSTRACT

We have used the Very Long Baseline Array at 15 GHz to image the structure of 132 strong compact active galactic nuclei (AGNs) and quasars with a resolution better than 1 mas and a dynamic range typically exceeding 1000:1. These observations were made as part of a program to investigate the subparsec structure of quasars and AGNs and to study the changes in their structure with time. Many of the sources included in our study, particularly those located south of declination $+35°$, have not been previously imaged with milliarcsecond resolution. Each of the sources has been observed at multiple epochs. In this paper, we show images of each of the 132 sources that we have observed. For each source we present data at the epoch that had the best quality data. In a future paper we will discuss the kinematics derived from the observations at all epochs.

Most of the sources we have observed show the canonical core-jet morphology with structure somewhat characteristic of the jets seen on arcsecond scales with the Very Large Array and Westerbork telescopes. The milliarcsecond jets generally appear one-sided, but two-sided structure is often found in lower luminosity radio galaxies and in high-luminosity quasars with gigahertz-peaked spectra. In many cases there is significant curvature, sometimes up to 90° or more, particularly close to the core. In other cases the jets have a more gradual curvature. In some sources there are multiple bends or twists along the jet, suggestive of a three-dimensional curved structure. Many of the jets may be described by a small number of apparently discrete components, but in other cases there appears to be a monotonically decreasing distribution of radio emission. Usually the structure is unresolved along the direction perpendicular to the jet, but a few sources have broad plumes. Much of the visible parsec-scale structure in compact radio sources can probably be explained as the projection of a relativistic beamed, twisted jet, which appears bright at those positions where it approaches the viewer. In some low-luminosity radio galaxies, the structure appears more symmetric at 2 cm than at longer wavelengths. The apparent long-wavelength asymmetry in these sources is probably due to absorption by intervening ionized material. A few sources contain only a single component, with any secondary feature at least 1000 times weaker. Peak rest-frame brightness temperatures are typically of the order of 10^{11}–10^{12} K, with no evidence for any excess over the limit of 10^{12} K expected from inverse Compton cooling. We find no obvious correlation of radio morphology and the detection of gamma-ray emission by EGRET.

Key words: galaxies: active — galaxies: jets — galaxies: nuclei

1. INTRODUCTION

Earlier VLBI studies have outlined the milliarcsecond structure of hundreds of compact radio sources with a resolution of about 1.5 mas. The most extensive observations of this type are from the series of Caltech–Jodrell Bank (CJ) surveys made at 1.6 and 5 GHz using antennas in Europe and the United States and covering more than 300 sources north of declination $+35°$ (Pearson & Readhead 1981, 1988; Taylor et al. 1994; Polatidis et al. 1995; Thakkar et al. 1995; Xu et al. 1995; Henstock et al. 1995; Taylor et al. 1996b).

The milliarcsecond (parsec scale) structure of quasars and active galactic nuclei (AGNs), at radio wavelengths, often appears one-sided with a linear extended feature, usually described as a "jet" (e.g., Zensus 1997). In the standard picture (Blandford & Rees 1974), however, the system is intrinsically symmetric, with twin oppositely directed jets containing relativistic beams. Differential Doppler boosting makes the approaching side appear much brighter than the receding component, and so the objects appear one-sided. A further effect is Doppler favoritism. Objects with jets oriented close to the line of sight have their flux density strongly Doppler boosted, and so they are preferentially found in flux-limited samples of sources chosen at centimeter wavelengths (e.g., Vermeulen & Cohen 1994). A great majority of the sources observed with milliarcsecond resolution show this one-sided morphology, but some objects are two-sided. Two-sided morphology can result when the axis is close to

[1] The National Radio Astronomy Observatory is a facility of the National Science Foundation operated under cooperative agreement by Associated Universities, Inc.

TABLE 1

SOURCE LIST

Source (1)	Name (2)	R.A. (J2000.0) (3)	Decl. (J2000.0) (4)	ID (5)	Magnitude (6)	z (7)	S_6 (Jy) (8)	EGRET? (9)
0003−066.....		00 06 13.893	−06 23 35.33	G	19.5	0.35	1.48	
0007+106.....	III Zw 2	00 10 31.007	10 58 29.51	G	15.4	0.09	0.43	
0016+731.....		00 19 45.787	73 27 30.02	Q	18.0	1.78	1.65	No
0026+346.....		00 29 14.244	34 56 32.26	G	20.7	0.52?	1.27	
0035+413.....		00 38 24.845	41 37 06.00	Q	19.1	1.35	1.11	
0048−097.....		00 50 41.317	−09 29 05.21	BL	17.4	...	1.98	
0055+300.....	NGC 315	00 57 48.887	30 21 08.84	G	12.2	0.02	1.18	
0106+013.....		01 08 38.771	01 35 00.32	Q	18.3	2.10	2.28	
0112−017.....		01 15 17.100	−01 27 04.58	Q	18.0	1.36	1.20	
0119+041.....		01 21 56.862	04 22 24.73	Q	19.5	0.64	1.67	
0133+476.....	DA 55	01 36 58.595	47 51 29.10	Q	18.0	0.86	3.22	
0149+218.....		01 52 18.060	22 07 07.70	Q	20.8	1.32	1.03	
0153+744.....		01 57 34.967	74 42 43.25	Q	16.0	2.34	1.52	No
0202+149.....		02 04 50.414	15 14 11.04	G?	22.1	...	2.47	
0202+319.....		02 05 04.926	32 12 30.10	Q	18.2	1.47	1.03	
0212+735.....		02 17 30.817	73 49 32.62	BL	19.0	2.37	2.20	No
0218+357.....		02 21 05.470	35 56 13.72	BL	20.0	1.00	1.16	
0234+285.....	CTD 20	02 37 52.406	28 48 08.99	Q	18.9	1.21	1.44	Yes
0235+164.....		02 38 38.931	16 36 59.28	BL	19.0	0.94	2.85	Yes
0238−084.....	NGC 1052	02 41 04.799	−08 15 20.75	G	11.4	0.00	1.44	
0316+162.....	CTA 21	03 18 57.760	16 28 32.34	Q	23.0	...	2.81	
0333+321.....	NRAO 140	03 36 30.108	32 18 29.34	Q	17.5	1.26	1.95	No
0336−019.....	CTA 26	03 39 30.938	−01 46 35.80	Q	18.4	0.85	2.86	Yes
0355+508.....	NRAO 150	03 59 29.748	50 57 50.16	EF	?	...	3.77	No
0415+379.....	3C 111	04 18 21.277	38 01 35.51	G	18.0	0.05	1.37	No
0420−014.....		04 23 15.801	−01 20 33.06	Q	17.8	0.92	1.46	Yes
0430+052.....	3C 120	04 33 11.096	05 21 15.63	G	14.2	0.03	8.44	No
0440−003.....	NRAO 190	04 42 38.660	00 17 43.47	Q	19.2	0.84	2.61	Yes
0454+844.....		05 08 42.363	84 32 04.54	BL	16.5	0.11	1.39	No
0458−020.....		05 01 12.810	−01 59 14.26	Q	18.4	2.29	1.74	Yes
0521−365.....		05 22 58.012	−36 27 31.90	G	14.5	0.06	9.29	Yes
0528+134.....		05 30 56.418	13 31 55.18	Q	20.0	2.06	3.97	Yes
0552+398.....	DA 193	05 55 30.806	39 48 49.16	Q	18.0	2.37	5.52	
0602+673.....		06 07 52.672	67 20 55.42	Q	20.6	1.97	1.06	
0605−085.....		06 07 59.699	−08 34 49.98	Q	18.5	0.87	3.49	No
0607−157.....		06 09 40.949	−15 42 40.67	Q	17.0	0.32	1.82	
0615+820.....		06 26 03.006	82 02 25.57	Q	17.5	0.71	1.00	No
0642+449.....	OH 471	06 46 32.026	44 51 16.59	Q	18.5	3.41	1.22	
0707+476.....		07 10 46.105	47 32 11.14	Q	18.2	1.29	1.01	
0710+439.....		07 13 38.177	43 49 17.00	G	19.7	0.52	1.67	
0716+714.....		07 21 53.449	71 20 36.36	BL	15.5	...	1.12	Yes
0727−115.....		07 30 19.112	−11 41 12.60	EF	?	...	2.2	
0735+178.....		07 38 07.394	17 42 19.00	BL	14.8	0.42	1.99	Yes
0736+017.....		07 39 18.034	01 37 04.62	Q	16.5	0.19	1.99	
0738+313.....		07 41 10.704	31 12 00.22	Q	16.1	0.63	2.49	
0742+103.....		07 45 33.060	10 11 12.69	EF	?	...	3.68	
0745+241.....		07 48 36.110	24 00 24.15	Q	18.5	0.41	1.01	
0748+126.....		07 50 52.047	12 31 04.83	Q	17.8	0.89	2.28	
0754+100.....		07 57 06.643	09 56 34.85	BL	14.5	0.66	0.90	
0804+499.....		08 08 39.667	49 50 36.53	Q	17.5	1.43	2.05	
0808+019.....		08 11 26.707	01 46 52.22	BL	17.5	...	1.40	
0814+425.....		08 18 16.000	42 22 45.41	BL	18.5	0.26	1.69	
0823+033.....		08 25 50.338	03 09 24.52	BL	18.5	0.51	1.32	
0829+046.....		08 31 48.878	04 29 39.08	BL	16.5	0.18	1.91	Yes
0850+581.....		08 54 41.991	57 57 29.95	Q	18.0	1.32	1.39	
0851+202.....	OJ 287	08 54 48.875	20 06 30.64	BL	14.0	0.31	2.62	
0859−140.....		09 02 16.831	−14 15 30.87	Q	16.6	1.33	2.30	
0917+449.....		09 20 58.459	44 41 53.98	Q	19.0	2.18	1.09	
0923+392.....	4C 39.25	09 27 03.014	39 02 20.85	Q	17.9	0.70	8.73	No
0945+408.....		09 48 55.339	40 39 44.58	Q	17.5	1.25	1.39	
0953+254.....		09 56 49.876	25 15 16.05	Q	17.5	0.71	1.82	
1012+232.....		10 14 47.067	23 01 16.57	Q	17.5	0.57	1.09	
1015+359.....		10 18 10.988	35 42 39.44	Q	19.0	1.23	0.71	
1049+215.....		10 51 48.790	21 19 52.35	Q	18.5	1.30	1.26	
1055+018.....		10 58 29.605	01 33 58.82	BL	18.3	0.89	3.47	
1055+201.....		10 58 17.902	19 51 50.90	Q	17.1	1.11	1.10	
1101+384.....	Mrk 421	11 04 27.315	38 12 31.79	G	13.3	0.03	0.72	Yes
1127−145.....		11 30 07.053	−14 49 27.39	Q	16.9	1.19	6.57	Yes
1128+385.....		11 30 53.282	38 15 18.55	Q	18.0	1.73	0.77	
1155+251.....		11 58 25.789	24 50 18.00	G	17.5	...	1.16	
1156+295.....	4C 29.45	11 59 31.834	29 14 43.82	Q	14.4	0.73	1.46	Yes

TABLE 1—*Continued*

Source (1)	Name (2)	R.A. (J2000.0) (3)	Decl. (J2000.0) (4)	ID (5)	Magnitude (6)	z (7)	S_6 (Jy) (8)	EGRET? (9)
1219+285.....		12 21 31.691	28 13 58.50	BL	16.5	0.10	1.09	Yes
1226+023.....	3C 273	12 29 06.700	02 03 08.60	Q	12.9	0.16	42.80	Yes
1228+126.....	M87	12 30 49.423	12 23 28.04	G	9.6	0.00	74.90	
1253−055.....	3C 279	12 56 11.167	−05 47 21.52	Q	17.8	0.54	14.90	Yes
1302−102.....		13 05 33.015	−10 33 19.43	Q	14.9	0.29	1.17	
1308+326.....		13 10 28.664	32 20 43.78	BL	19.0	1.00	1.53	
1323+321.....		13 26 16.514	31 54 09.52	G	19.0	0.37	2.28	
1328+254.....	3C 287	13 30 37.690	25 09 11.00	Q	17.7	1.06	3.22	
1328+307.....	3C 286	13 31 08.287	30 30 32.96	Q	17.2	0.85	7.40	
1334−127.....		13 37 39.783	−12 57 24.69	BL	17.2	0.54	2.24	
1404+286.....	OQ 208	14 07 00.395	28 27 14.69	G	16.0	0.08	2.95	
1413+135.....		14 15 58.819	13 20 23.71	BL	20.0	0.26	0.85	
1424+366.....		14 26 37.088	36 25 09.59	BS	18.3	1.09	0.43	
1508−055.....		15 10 53.552	−05 43 06.40	Q	17.2	1.18	2.43	
1510−089.....		15 12 50.533	−09 05 59.83	Q	16.5	0.36	3.08	Yes
1532+016.....		15 34 52.454	01 31 04.21	Q	18.7	1.44	1.14	
1546+027.....		15 49 29.437	02 37 01.16	Q	18.0	0.41	1.45	
1548+056.....		15 50 35.270	05 27 10.47	Q	17.7	1.42	2.24	
1606+106.....		16 08 46.204	10 29 07.78	Q	18.5	1.23	1.49	Yes
1611+343.....	DA 406	16 13 41.064	34 12 47.91	Q	17.5	1.40	2.67	Yes
1633+382.....		16 35 15.493	38 08 04.50	Q	18.0	1.81	4.02	Yes
1638+398.....	NRAO 512	16 40 29.633	39 46 46.03	Q	18.5	1.66	1.15	
1641+399.....	3C 345	16 42 58.810	39 48 36.99	Q	16.0	0.59	10.80	No
1642+690.....		16 42 07.849	68 56 39.76	Q	19.2	0.75	1.39	No
1652+398.....	Mrk 501	16 53 52.217	39 45 36.61	G	14.2	0.03	1.42	
1655+077.....		16 58 09.011	07 41 27.54	Q	20.8	0.62	1.65	
1656+053.....		16 58 33.447	05 15 16.44	Q	16.5	0.89	2.16	
1656+477.....		16 58 02.779	47 37 49.24	Q	18.0	1.62	1.24	
1730−130.....	NRAO 530	17 33 02.706	−13 04 49.55	Q	18.5	0.90	...	Yes
1741−038.....		17 43 58.856	−03 50 04.62	Q	18.6	1.05	3.68	
1749+096.....		17 51 32.819	09 39 00.73	BL	16.8	0.32	1.87	
1749+701.....		17 48 32.840	70 05 50.77	BL	17.0	0.77	1.45	No
1758+388.....		18 00 24.765	38 48 30.70	Q	18.0	2.09	0.74	
1800+440.....		18 01 32.315	44 04 21.90	Q	17.5	0.66	1.10	
1803+784.....		18 00 45.684	78 28 04.02	BL	17.0	0.68	2.62	No
1807+698.....	3C 371	18 06 50.681	69 49 28.11	BL	14.4	0.05	2.26	No
1823+568.....		18 24 07.068	56 51 01.49	BL	18.4	0.66	1.66	
1845+797.....	3C 390.3	18 42 08.990	79 46 17.13	G	14.4	0.06	4.38	No
1901+319.....	3C 395	19 02 55.935	31 59 41.64	Q	17.5	0.64	1.87	No
1921−293.....	OV 236	19 24 51.056	−29 14 30.12	Q	17.0	0.35	10.60	
1928+738.....		19 27 48.495	73 58 01.57	Q	16.5	0.30	3.34	No
1957+405.....	Cyg A	19 59 28.348	40 44 02.02	G	?	0.06	0.75	
2005+403.....		20 07 44.945	40 29 48.61	Q	19.5	1.74	3.70	
2007+776.....		20 05 31.010	77 52 43.21	BL	16.5	0.34	1.26	No
2021+317.....		20 23 19.018	31 53 02.31	?	?	...	3.05	
2021+614.....		20 22 06.682	61 36 58.81	G	19.5	0.23	2.31	
2113+293.....		21 15 29.414	29 33 38.37	Q	19.5	1.514?	1.47	
2131−021.....		21 34 10.310	−01 53 17.24	BL	18.7	0.56	2.12	
2134+004.....		21 36 38.586	00 41 54.20	Q	16.8	1.93	12.30	No
2136+141.....		21 39 01.310	14 23 35.99	Q	18.5	2.43	1.11	
2144+092.....		21 47 10.163	09 29 46.68	Q	18.9	1.11	1.01	
2145+067.....		21 48 05.459	06 57 38.61	Q	16.5	0.99	4.40	
2200+420.....	BL Lac	22 02 43.292	42 16 39.98	BL	14.5	0.07	4.77	Yes
2201+315.....		22 03 14.976	31 45 38.27	Q	15.5	0.30	2.32	
2209+236.....		22 12 05.968	23 55 40.59	Q	19.0	...	1.12	Yes
2223−052.....	3C 446	22 25 47.259	−04 57 01.39	BL	17.2	1.40	4.51	No
2230+114.....	CTA 102	22 32 36.409	11 43 50.89	Q	17.3	1.04	3.61	Yes
2234+282.....		22 36 22.471	28 28 57.42	Q	19.0	0.80	1.06	
2243−123.....		22 46 18.232	−12 06 51.28	Q	16.4	0.63	2.45	
2251+158.....	3C 454.3	22 53 57.748	16 08 53.56	Q	16.1	0.86	17.40	Yes
2345−167.....		23 48 02.609	−16 31 12.02	Q	17.5	0.58	3.36	

the plane of the sky or when the beam velocity is subrelativistic, so that the Doppler boosting is small. Most of these two-sided sources have large-scale structure, but there is a class of symmetric sources that do not extend beyond 1 kpc. These are referred to as "compact symmetric objects" (CSOs; e.g., Wilkinson et al. 1994; Readhead et al. 1996b).

In this paper, we report on the first part of a source survey being made with the NRAO Very Long Baseline Array (VLBA; Napier et al. 1994) at a frequency of 15 GHz (2 cm) with a nominal resolution of 0.5 mas (4 pc at moderate redshift), in the east-west direction and between 0.6 and 1.3 mas in declination, and with a sensitivity of 200–300 μJy rms noise. This is the shortest wavelength and highest resolution that have been used to images a large sample of radio sources. Typically the dynamic range (defined as peak to rms noise) of our images is better than 1000:1, but for the

weaker sources it is limited by receiver noise. Throughout this paper we adopt $H_0 = 65$ km s^{-1} Mpc^{-1} and $q_0 = 0.5$.

The observations reported here are part of an extended program to study motions and other time variations in source morphology. We show here the structure of each source in our program from one epoch of observation, selected as the one with the best quality data.[2]

We have exploited the good two-dimensional coverage of the VLBA to image sources as far south as $-20°$ declination with good image quality, and as far south as $-40°$ for a few strong sources. These are the first observations ever made of the subarcsecond structure of many of the sources south of declination $+35°$. At declinations north of $+35°$, many sources have also been observed as part of the CJ 6 and 18 cm surveys.

Our resolution at 2 cm is improved by about a factor of 2–3 over the Caltech-Jodrell 6 cm global observations. Our 2 cm VLBA images have a resolution comparable to that which will be obtained from the *HALCA* space VLBI mission at 6 cm, but the 2 cm VLBA images have considerably better sensitivity and dynamic range. Generally, our observing frequency is above the synchrotron self-absorption turnover frequency; thus our observations penetrate further into the nuclear regions than VLBI observations made at lower frequencies.

Our goals were to classify and study the morphological characteristics of compact radio sources; to examine the relation between radio structure and luminosity, spectra, optical counterparts, and redshift; to search for structures that might indicate gravitational minilensing; to find unresolved or nearly unresolved sources to use as VLBA calibrators; and to examine the spectral distribution on parsec scales. In addition to the CJ 6 and 18 cm observations of sources north of declination $+35°$, many of these sources have also been observed with lower resolution and sensitivity as part of astrometric surveys made at 3.6 and 13 cm (Fey, Clegg, & Fomalont 1996; Fey & Charlot 1997; Peck & Beasley 1998). Comparison of these longer wavelength images with our 2 cm images will yield information on the spectral distribution across individual sources. Also, as the images at these longer wavelengths are generally more sensitive to the larger lower surface brightness structure, comparison of images over a range of wavelengths allows the structure to be traced over a wider range of sizes than is possible at a single VLBA wavelength.

In this paper, we discuss our observing procedures, then present and discuss the images. These images serve as a finding list for those interested in more extensive observing programs. Further analysis and discussion are deferred to later papers.

2. SOURCE SAMPLE

Our sample of sources listed in Table 1 is based on the complete 5 GHz 1 Jy catalog of Kühr et al. (1981) as supplemented by Stickel, Meisenheimer, & Kühr (1994). Table 1 is organized as follows:

Column (*1*).—IAU source designation.

Column (*2*).—Alternative source name where appropriate.

Columns (*3*) *and* (*4*).—Right ascension and declination (J2000.0).

Column (*5*).—The optical counterpart, denoted as follows: (G) galaxy, (Q) quasar, (BL) BL Lac object, or (EF) empty field.

Column (*6*).—Optical magnitude.

Column (*7*).—Redshift.

Column (*8*).—Flux density at 5 GHz, taken mostly from Stickel et al. (1994).

Column (*9*).—Indication of whether the source has been detected by the EGRET instrument on the *Compton Gamma Ray Observatory* (Mattox et al. 1997) or not detected (von Montigny et al. 1995b).

Our goal was to include all known sources in the Stickel et al. catalog with spectral index, α, flatter than -0.5 ($S \propto \nu^{\alpha}$) at any frequency above 500 MHz and with a measured or extrapolated flux density at 15 GHz greater than 1.5 Jy for sources north of the equator or greater than 2 Jy for sources between declinations $-20°$ and the equator. Scheduling constraints did not allow us to include all sources meeting these criteria, but also allowed some weaker sources to be included in the observing schedule. As it turned out, our measurements show that many of the sources we observed had integrated flux densities considerably lower than expected. This is due to variability, as well as to uncertainties in the earlier flux density measurements. We have not included known gravitationally lensed sources, except for 0218+357.

In estimating the 15 GHz flux density, we used data taken from VLA measurements listed in the NRAO VLA Calibrator Manual, from the University of Michigan observations made available by M. F. Aller & H. D. Aller,[3] from published spectra (Kühr et al. 1981; Xu et al. 1995; Herbig & Readhead 1995) and unpublished spectra observed by Yu. A. Kovalev (1977, private communication) with the RATAN-600 radio telescope, and from the interpolation and extrapolation of measurements at nearby frequencies when 15 GHz observations were not available. Optical counterparts, magnitudes, and redshifts were compiled from a variety of literature sources with the aid of the NASA/IPAC Extragalactic Database.

3. OBSERVING PROCEDURE

The observations were made during eight observing sessions between 1994 and 1997, as summarized in Table 2. In order to optimize the *u-v* coverage, we observed each source over a wide range of hour angle. We deleted data taken from any antenna when its elevation was below 10° or during periods of excessively bad weather when the excess sky temperature exceeded 75 K, or was changing very rapidly because of heavy rain or thick cloud cover. In Figure 1, we show the typical *u-v* coverage for four sources located over a range of declinations.

We observed with a bandwidth of 64 MHz (32 MHz in 1994) using 1 bit samples and left-circular polarization. Each source was observed for 4–5 minutes once each hour for a range of 8 hours (12 in 1994). Thus we observed three such groups per day (two in 1994), for a nominal total of 27 sources per day (18 in 1994) at the low (33 kbit inch^{-1}) bit density and 30 sources per day at the high (56 kbit inch^{-1}) bit density. The rms noise in each image was typically about 400 μJy for the high-declination sources observed in 1994

[2] Images at this and other epochs are available on the World Wide Web at http://www.cv.nrao.edu/2cmsurvey, and future observations will be included at this site as they become available.

[3] See http://www.astro.lsa.umich.edu/obs/radiotel/umrao.html.

TABLE 2

LOG OF OBSERVATIONS

Date (1)	Bit Rate (Mbit s^{-1}) (2)	Linear Bit Density (kbit $inch^{-1}$) (3)	Frequency Channels (4)	Integration Time[a] (5)	Sources (6)
1994 Aug 31	64	33	8	60	18
1995 Apr 4–6.....	128	33	16	30	52
1995 Jul 28–30	128	33	16	30	53
1995 Dec 15–17	128	33	16	30	54
1996 May 18	128	56	16	30	33
1996 Jul 10–11	128	56	16	30	28
1996 Oct 27–29	128	56	16	30	58
1997 Mar 10–14.....	128	56	256	30	55

[a] Per source, in minutes.

and 200–300 μJy for the other observations, about that expected from the nominal system temperature of 60–100 K and antenna gain of about 0.1 K Jy^{-1}.

Table 2 shows the log of our observations, with the epoch given in column (1), the bit rate in column (2), the linear bit density recorded on tape in kbit $inch^{-1}$ in column (3), the number of intermediate frequency (IF) channels in column (4), the approximate total observing time per source in column (5), and the number of sources observed in column (6).

The VLBA uses an FX correlator, which gave us between eight and 256 frequency channels in each of four to eight IF

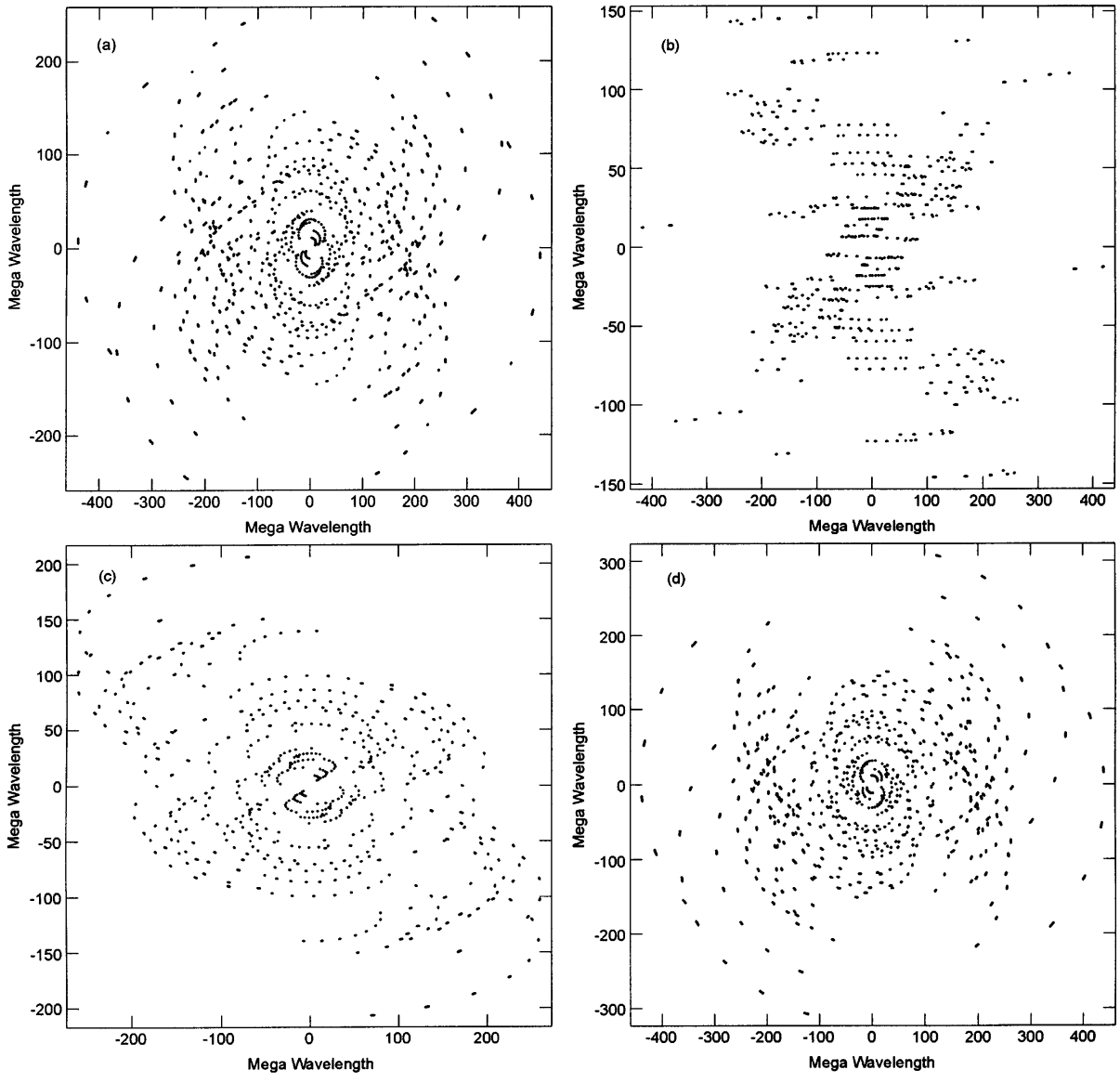

FIG. 1.—Plots showing typical u-v coverage for survey sources over a range of declinations: (*a*) 1127−145; (*b*) 2134+004; (*c*) 2251+158; (*d*) 1641+399

bands. The differential delays across each IF band and between bands were calibrated by observations of a strong source during each observing session. We then made a conventional global fringe fit to the data before determining the amplitude and phase of the visibilities. The VLBA is quite stable with time: fringe rates and delays were normally constant to within a few millihertz and a few nanoseconds, respectively. Data from the Hancock and St. Croix sites typically showed larger phase variations due to the significantly greater water vapor column above these antennas.

Initial editing, amplitude calibration using the nominal gain curves determined for each antenna, and fringe fitting were performed using the standard NRAO AIPS package. After averaging over frequency, further editing for deviant data points was carried out using the Caltech DIFMAP package, and an automated DIFMAP procedure was used for imaging (Shepherd, Pearson, & Taylor 1994a, 1994b)

Starting with visibility phases self-calibrated with a point-source model, the DIFMAP procedure alternates between searches for new CLEAN image components and self-calibration. All CLEANing takes place on the residual image, formed from the difference between the observed visibilities and the model as established up to that point. For each CLEAN cycle, we made 100 iterations with a loop gain of 0.03. Before each cycle, one new CLEAN window is automatically placed around the highest peak in the current residual image, as long as this peak exceeds 7–9 times the current rms image noise. The specific threshold factor was determined experimentally on a few test sources prior to batch-processing each observing run, and varied with the data quality. The shape of the rectangular windows is chosen to be an optimal match to the beam shape, and to have an area of 10–20 independent beam areas as determined from a few test sources imaged prior to batch processing.

The initial cycles are performed using uniform weighting of the data over 2×2 (u, v) grid points. When convergence is reached (no more new peaks meriting a new window and no more flux density to be CLEANed within the windows above 3 times the rms noise), the weighting changes to natural, and the threshold for placing new windows is lowered to 5–7 times the residual image rms noise. When this, in turn, converges, self-calibration of amplitudes, as well as phases, is enabled, first by allowing one gain factor per antenna for the entire observation, later by solving for amplitude gains in 30 minute intervals, and finally by having separate solutions for each integration, but only when the peak flux density exceeds the experimentally determined threshold of 0.5 Jy.

With this automated procedure, we nearly reached the theoretical noise floor for most sources. For about 25% of the sources, which had unusually complex structure, were sufficiently strong, or otherwise had inadequate u-v coverage, the above procedure did not result in noise-limited images. For these sources we made further iterations of the CLEAN self-calibration loop using manually determined parameters.

The resulting images have a nominal resolution of about 0.5 mas along the minor axis, and from 0.6 to 1 mas along the major axis, except for sources near the equator, where the major axis is as large as 1.3 mas. Most images are 25.6 mas on a side. In addition to the full-resolution images, we examined an image for each source convolved to yield a circular beam with resolution of 1.5 mas. We inspected each of these lower resolution images for structure over an area of 51.2 mas on a side. For sources in which there was evidence for additional emission from other observations, or in which such emission was suggested to be present by our inability to fit the data, we searched a larger area.

4. SOURCE STRUCTURE

In Table 3, we summarize the images and give a guide to the contour maps shown in Figure 2. Table 3 is organized as follows:

Column (*1*).—IAU source designation.

Column (*2*).—Total flux density in janskys at 15 GHz measured from our images.

Column (*3*).—Monochromatic luminosity at 15 GHz in the rest frame of the source, calculated assuming a spectral index of zero and isotropic radiation. As we believe most of these sources are relativistically boosted, the true luminosity is probably smaller by a factor of 10–100.

Column (*4*).—Epoch of the VLBA image shown in Figure 2.

Column (*5*).—Lowest contour level of the image Figure 2, which is 3 times the rms noise in the image.

Columns (*6*)–(*8*).—Major axis, minor axis, and position angle of the CLEAN beam in milliarcseconds.

Column (*9*).—Peak flux density in janskys per beam measured from the VLBA image.

Column (*10*).—Peak brightness temperature in the source rest frame calculated from the following expression: $T_b = 7.6 \times 10^{10} S_{\rm peak}(1 + z)/(\theta_{\rm maj}\,\theta_{\rm min})$, where $S_{\rm peak}$ is the peak flux density in janskys per beam and $\theta_{\rm maj}$ and $\theta_{\rm min}$ are the semimajor and semiminor axes of the beam, respectively. In the few cases where no redshift is available, we set $z = 0$.

Column (*11*).—Classification of the structure, as follows: (C) compact, (SS) single-sided, (DS) double-sided, or (Irr) irregular, as described below.

In Figure 2, we show a contour map for each source. Figure 3 shows false-color images for six sources indicating the range of structures that are observed.

Pearson & Readhead (1988) have classified the structure of the sources in their pioneering 5 GHz VLBI survey into 10 categories and subcategories, most of which exhibited pronounced asymmetry. Later, Wilkinson et al. (1994) called attention to the class of compact symmetric objects (CSOs). More recently, Wilkinson (1995) has described all sources as either core-jets, with a wide range of core/jet strengths, jet lengths, and jet bends, or CSOs. Since many of the so-called parsec-scale jets do not meet the 4:1 length-to-thickness ratio specified by Bridle & Perley (1984) to define a jet, and so as not to prejudice the interpretation of the underlying physics, we chose to classify each source as either having a compact (C), e.g., barely resolved appearance; a single-sided (SS) or double-sided (DS) appearance, depending on whether the most compact component is located on one side or is in the middle; or an irregular (Irr) two-dimensional structure.

We note that many of the sources reported here appear to have smooth secondary features or otherwise have complex structures, and we have chosen not to try to describe our images in terms of individual components that may not have any physical reality. Comments on individual sources are given in the next section. We have not made an exhaustive search of the literature to document previous observations of these sources. Rather, we comment on peculiarities of the radio structure, observations at other

TABLE 3

SOURCE STRUCTURE

Source	S_{total} (Jy)	Luminosity (W Hz^{-1})	Epoch	Contour (mJy)	θ_{maj} (mas)	θ_{min} (mas)	P.A. (deg)	S_{peak} (Jy beam^{-1})	T_b (K)	Structure
0003−066.....	1.92	5.1×10^{26}	1996 Oct	2.1	1.1	0.5	−4	1.21	2.25×10^{10}	SS
0007+106.....	0.10	1.9×10^{24}	1997 Mar	0.6	1.1	0.6	−1	0.10	1.21×10^{9}	DS
0016+731.....	0.70	3.2×10^{27}	1996 Jul	1.6	0.8	0.6	12	0.32	1.42×10^{10}	C
0026+346.....	0.65	3.6×10^{26}	1995 Apr	0.9	0.9	0.5	12	0.10	2.61×10^{9}	DS
0035+413.....	0.41	1.2×10^{27}	1996 Jul	1.0	0.9	0.5	4	0.26	1.01×10^{10}	SS
0048−097.....	1.34	...	1995 Jul	1.3	1.2	0.5	0	1.30	1.64×10^{10}	C
0055+300.....	0.69	4.7×10^{23}	1995 Dec	0.9	0.9	0.5	−6	0.35	6.00×10^{9}	SS
0106+013.....	1.34	7.9×10^{27}	1997 Mar	1.0	1.1	0.5	0	1.01	4.28×10^{10}	SS
0112−017.....	0.82	2.4×10^{27}	1995 Jul	1.4	1.2	0.5	4	0.40	1.19×10^{10}	SS
0119+041.....	1.27	1.0×10^{27}	1995 Jul	1.1	1.1	0.5	0	0.98	2.20×10^{10}	SS
0133+476.....	2.22	3.0×10^{27}	1997 Mar	1.9	0.9	0.6	−1	1.98	5.14×10^{10}	SS
0149+218.....	1.42	4.0×10^{27}	1995 Dec	1.2	1.1	0.5	0	1.26	4.03×10^{10}	SS
0153+744.....	0.37	2.6×10^{27}	1996 Jul	1.3	0.8	0.5	29	0.19	1.22×10^{10}	SS
0202+149.....	2.29	...	1995 Jul	2.1	1.1	0.5	1	1.80	2.47×10^{10}	SS
0202+319.....	1.11	3.7×10^{27}	1997 Mar	1.3	0.9	0.5	0	1.03	4.27×10^{10}	SS
0212+735.....	2.69	1.9×10^{28}	1994 Aug	2.3	0.7	0.6	−69	2.14	1.30×10^{11}	SS
0218+357.....	1.14	2.0×10^{27}	1995 Apr	1.7	0.9	0.5	1	0.44	1.47×10^{10}	...
0234+285.....	1.56	3.8×10^{27}	1995 Dec	1.6	1.0	0.5	2	1.07	3.57×10^{10}	SS
0235+164.....	0.79	1.2×10^{27}	1995 Jul	1.1	1.0	0.6	1	0.67	1.64×10^{10}	C
0238−084.....	2.08	1.3×10^{23}	1997 Mar	1.0	1.2	0.5	0	0.36	4.50×10^{9}	DS
0316+162.....	0.34	...	1997 Mar	0.8	3.0	2	−11	0.14	1.74×10^{8}	Irr
0333+321.....	1.26	3.2×10^{27}	1997 Mar	1.1	1.0	0.5	5	0.86	2.95×10^{10}	SS
0336−019.....	2.23	3.0×10^{27}	1997 Mar	1.0	1.2	0.5	2	1.73	4.04×10^{10}	SS
0355+508.....	3.23	...	1995 Apr	1.2	0.8	0.5	14	2.70	5.11×10^{10}	SS
0415+379.....	5.98	3.5×10^{25}	1997 Mar	4.8	0.9	0.6	−3	2.28	3.35×10^{10}	SS
0420−014.....	4.20	6.3×10^{27}	1995 Jul	2.4	1.2	0.5	−1	3.56	8.60×10^{10}	SS
0430+052.....	3.01	8.2×10^{24}	1997 Mar	1.9	1.1	0.5	1	1.10	1.56×10^{10}	SS
0440−003.....	1.04	1.4×10^{27}	1995 Jul	1.9	1.2	0.5	2	0.61	1.41×10^{10}	SS
0454+844.....	0.30	9.1×10^{24}	1994 Aug	1.2	0.7	0.7	−35	0.23	3.93×10^{9}	SS
0458−020.....	2.33	1.6×10^{28}	1995 Jul	2.5	1.2	0.6	5	1.89	6.51×10^{10}	SS
0521−365.....	2.15	1.6×10^{25}	1995 Jul	1.6	3.4	0.7	19	1.52	5.10×10^{9}	SS
0528+134.....	7.95	4.6×10^{28}	1995 Jul	7.4	1.1	0.6	5	6.95	2.44×10^{11}	SS
0552+398.....	5.02	3.6×10^{28}	1997 Mar	3.1	1.0	0.5	6	3.68	1.87×10^{11}	SS
0602+673.....	0.50	2.7×10^{27}	1994 Aug	1.3	0.7	0.6	−45	0.42	2.25×10^{10}	SS
0605−085.....	2.80	3.9×10^{27}	1995 Jul	3.0	1.2	0.5	2	2.02	4.75×10^{10}	SS
0607−157.....	5.60	1.3×10^{27}	1995 Jul	4.9	1.3	0.5	0	4.62	7.11×10^{10}	SS
0615+820.....	0.39	3.8×10^{26}	1996 Jul	1.2	0.8	0.5	−25	0.17	5.43×10^{9}	Irr
0642+449.....	2.09	2.6×10^{28}	1995 Apr	2.6	0.9	0.5	5	1.73	1.28×10^{11}	C
0707+476.....	0.41	1.1×10^{27}	1996 Jul	1.2	0.8	0.5	−10	0.31	1.34×10^{10}	SS
0710+439.....	0.50	2.7×10^{26}	1996 Oct	0.5	0.9	0.6	22	0.11	2.32×10^{9}	DS
0716+714.....	0.25	...	1996 Jul	0.9	0.8	0.5	−16	0.23	4.29×10^{9}	SS
0727−115.....	2.17	...	1995 Jul	2.3	1.2	0.5	1	1.62	2.05×10^{10}	SS
0735+178.....	0.69	2.6×10^{26}	1997 Mar	1.2	1.1	0.6	9	0.33	5.43×10^{9}	SS
0736+017.....	2.58	2.2×10^{26}	1995 Jul	1.4	1.2	0.5	9	2.06	3.09×10^{10}	SS
0738+313.....	1.94	1.5×10^{27}	1995 Apr	1.6	1.0	0.5	8	0.80	1.97×10^{10}	SS
0742+103.....	1.34	...	1997 Mar	1.1	1.1	0.6	10	0.51	5.82×10^{9}	SS
0745+241.....	0.64	2.3×10^{26}	1997 Mar	0.7	1.0	0.5	8	0.47	9.96×10^{9}	SS
0748+126.....	3.25	4.6×10^{27}	1997 Mar	2.1	1.1	0.6	7	2.77	6.00×10^{10}	SS
0754+100.....	1.50	1.3×10^{27}	1997 Mar	1.3	1.1	0.6	1	1.12	2.12×10^{10}	SS
0804+499.....	0.60	1.9×10^{27}	1997 Mar	0.8	0.9	0.6	−11	0.51	1.74×10^{10}	SS
0808+019.....	1.34	...	1995 Jul	1.2	1.2	0.5	−1	1.32	1.66×10^{10}	C
0814+425.....	0.90	1.4×10^{26}	1995 Apr	0.9	0.9	0.5	12	0.54	1.15×10^{10}	SS
0823+033.....	1.25	6.6×10^{26}	1995 Jul	1.4	1.2	0.6	−5	0.97	1.54×10^{10}	SS
0829+046.....	0.97	7.4×10^{25}	1996 Oct	1.0	1.0	0.4	−7	0.61	1.35×10^{10}	SS
0850+58	0.54	1.5×10^{27}	1995 Dec	1.0	0.9	0.5	17	0.30	1.19×10^{10}	SS
0851+202.....	1.16	2.4×10^{26}	1997 Mar	1.2	1.0	0.6	1	0.84	1.38×10^{10}	SS
0859−140.....	1.58	4.5×10^{27}	1995 Jul	0.8	1.2	0.5	1	1.14	3.35×10^{10}	SS
0917+449.....	1.10	6.9×10^{27}	1997 Mar	0.9	0.9	0.5	−1	0.70	3.75×10^{10}	SS
0923+392.....	10.84	1.0×10^{28}	1997 Mar	10.2	0.9	0.6	−1	7.20	1.71×10^{11}	SS
0945+408.....	1.37	3.5×10^{27}	1995 Apr	1.4	1.1	0.5	−14	0.81	2.50×10^{10}	SS
0953+254.....	1.31	1.3×10^{27}	1996 May	1.7	0.9	0.5	−3	0.69	1.98×10^{10}	SS
1012+232.....	1.00	6.4×10^{26}	1995 Apr	1.3	1.2	0.5	−12	0.76	1.49×10^{10}	SS
1015+359.....	0.51	1.3×10^{27}	1997 Mar	0.8	0.9	0.6	2	0.43	1.34×10^{10}	SS
1049+215.....	1.04	2.8×10^{27}	1997 Mar	1.0	1.0	0.5	3	0.70	2.44×10^{10}	SS
1055+018.....	2.15	3.1×10^{27}	1996 Oct	3.4	1.0	0.5	−3	1.57	4.49×10^{10}	SS
1055+201.....	0.32	6.7×10^{26}	1995 Dec	0.8	1.0	0.6	7	0.20	5.45×10^{9}	SS
1101+384.....	0.52	1.2×10^{24}	1997 Mar	0.7	0.9	0.5	5	0.44	7.70×10^{9}	SS
1127−145.....	2.03	4.7×10^{27}	1997 Mar	1.9	1.4	0.6	7	1.00	1.98×10^{10}	SS
1128+385.....	0.87	3.8×10^{27}	1995 Apr	1.3	1.2	0.5	−8	0.75	2.58×10^{10}	SS
1155+251.....	0.24	...	1995 Apr	1.1	1.0	0.5	−1	0.10	1.44×10^{9}	Irr
1156+295.....	1.01	1.0×10^{27}	1997 Mar	1.0	0.9	0.5	11	0.67	1.96×10^{10}	SS
1219+285.....	0.43	1.1×10^{25}	1995 Apr	1.2	1.0	0.5	−5	0.20	3.35×10^{9}	SS

TABLE 3—*Continued*

Source	S_{total} (Jy)	Luminosity (W Hz^{-1})	Epoch	Contour (mJy)	θ_{maj} (mas)	θ_{min} (mas)	P.A. (deg)	S_{peak} (Jy beam^{-1})	T_b (K)	Structure
1226+023.....	25.72	1.5×10^{27}	1997 Mar	8.6	1.1	0.5	0	9.18	1.46×10^{11}	SS
1228+126.....	2.40	1.1×10^{23}	1997 Mar	0.8	1.1	0.6	0	1.12	1.29×10^{10}	SS
1253−055.....	21.56	1.3×10^{28}	1997 Mar	4.8	1.2	0.5	1	15.43	2.99×10^{11}	SS
1302−102.....	0.70	1.3×10^{26}	1995 Jul	1.3	1.2	0.5	0	0.54	8.72×10^{9}	SS
1308+326.....	3.31	5.8×10^{27}	1996 May	4.9	0.9	0.5	−8	2.09	7.02×10^{10}	C
1323+321.....	0.65	1.9×10^{26}	1995 Apr	0.8	1.1	0.4	20	0.04	9.42×10^{8}	DS
1328+254.....	0.08	1.5×10^{26}	1995 Apr	2.3	0.9	0.4	2	0.09	3.76×10^{9}	...
1328+307.....	0.78	1.0×10^{27}	1997 Mar	1.4	2.6	1.7	21	0.17	5.28×10^{8}	Irr
1334−127.....	5.10	3.0×10^{27}	1995 Jul	3.7	1.3	0.5	1	4.64	8.31×10^{10}	SS
1404+286.....	0.97	1.4×10^{25}	1995 Dec	1.2	1.0	0.5	1	0.61	9.95×10^{9}	DS
1413+135.....	1.58	2.4×10^{26}	1995 Jul	1.6	1.0	0.5	3	1.41	2.68×10^{10}	SS
1424+366.....	0.43	8.7×10^{26}	1997 Mar	0.7	1.0	0.6	13	0.30	7.93×10^{9}	SS
1508−055.....	0.73	1.7×10^{27}	1997 Mar	0.7	1.2	0.5	7	0.54	1.49×10^{10}	SS
1510−089.....	1.20	3.4×10^{26}	1995 Jul	2.5	1.4	0.6	13	0.74	9.09×10^{9}	SS
1532+016.....	0.76	2.4×10^{27}	1997 Mar	0.8	1.1	0.5	6	0.36	1.20×10^{10}	Irr
1546+027.....	2.83	1.0×10^{27}	1996 Oct	3.2	1.0	0.5	−2	2.64	5.63×10^{10}	SS
1548+056.....	2.83	8.9×10^{27}	1997 Mar	0.9	1.1	0.5	6	2.10	6.98×10^{10}	SS
1606+106.....	1.56	3.9×10^{27}	1997 Mar	1.1	1.1	0.5	8	1.23	3.77×10^{10}	SS
1611+343.....	4.05	1.2×10^{28}	1997 Mar	1.9	0.9	0.5	17	2.72	1.10×10^{11}	Irr
1633+382.....	1.40	6.5×10^{27}	1997 Mar	1.5	1.0	0.6	−6	0.73	2.59×10^{10}	SS
1638+398.....	0.98	4.0×10^{27}	1995 Apr	1.1	0.9	0.5	−6	0.78	3.49×10^{10}	C
1641+399.....	8.48	5.9×10^{27}	1995 Apr	2.3	0.9	0.5	−5	4.53	1.21×10^{11}	SS
1642+690.....	0.63	6.7×10^{26}	1996 Jul	1.1	0.7	0.5	3	0.36	1.38×10^{10}	SS
1652+398.....	0.77	2.2×10^{24}	1997 Mar	0.4	0.9	0.5	−7	0.38	6.59×10^{9}	SS
1655+077.....	1.73	1.3×10^{27}	1997 Mar	1.6	1.2	0.5	−4	1.40	2.87×10^{10}	SS
1656+053.....	0.46	6.6×10^{26}	1996 Jul	1.6	1.2	0.6	−5	0.26	5.25×10^{9}	SS
1656+477.....	1.05	4.1×10^{27}	1997 Mar	0.9	0.9	0.5	−7	0.66	2.90×10^{10}	SS
1730−130.....	9.88	1.4×10^{28}	1995 Jul	3.4	1.4	0.6	3	8.79	1.51×10^{11}	SS
1741−038.....	4.06	7.8×10^{27}	1995 Jul	2.7	1.3	0.6	6	3.77	7.52×10^{10}	C
1749+096.....	5.58	1.3×10^{27}	1995 Jul	3.5	1.2	0.6	10	5.49	7.63×10^{10}	SS
1749+701.....	0.55	6.1×10^{26}	1997 Mar	0.7	0.8	0.5	−5	0.40	1.35×10^{10}	SS
1758+388.....	1.43	8.4×10^{27}	1995 Apr	1.6	0.9	0.5	3	1.22	6.34×10^{10}	SS
1800+440.....	1.02	8.7×10^{26}	1997 Mar	0.9	0.9	0.5	−1	0.93	2.60×10^{10}	SS
1803+784.....	2.05	1.8×10^{27}	1997 Mar	1.1	0.8	0.5	−5	1.46	4.63×10^{10}	SS
1807+698.....	1.13	7.3×10^{24}	1997 Mar	0.8	0.8	0.5	−3	0.66	1.31×10^{10}	SS
1823+568.....	2.31	2.0×10^{27}	1995 Dec	1.4	0.9	0.5	3	2.05	5.73×10^{10}	SS
1845+797.....	0.37	2.9×10^{24}	1997 Mar	0.6	0.8	0.5	4	0.18	3.57×10^{9}	SS
1901+319.....	1.09	8.6×10^{26}	1997 Mar	1.1	1.0	0.6	−10	0.64	1.33×10^{10}	SS
1921−293.....	14.39	3.9×10^{27}	1995 Jul	14.4	1.8	0.6	17	9.57	9.06×10^{10}	SS
1928+738.....	3.04	6.2×10^{26}	1996 Oct	3.2	0.7	0.5	16	1.15	3.24×10^{10}	SS
1957+405.....	1.68	1.3×10^{25}	1995 Dec	1.5	1.0	0.5	9	0.60	9.52×10^{9}	DS
2005+403.....	2.51	1.1×10^{28}	1997 Mar	2.8	0.9	0.5	−8	1.02	4.69×10^{10}	SS
2007+777.....	1.05	2.7×10^{26}	1995 Dec	1.7	0.8	0.5	−14	0.61	1.55×10^{10}	SS
2021+317.....	2.02	...	1996 May	3.3	0.9	0.5	−14	1.13	1.90×10^{10}	DS
2021+614.....	2.21	2.6×10^{26}	1995 Dec	2.6	0.9	0.5	−8	1.19	2.45×10^{10}	SS
2113+293.....	0.94	3.3×10^{27}	1995 Apr	2.1	0.9	0.5	−1	0.87	3.66×10^{10}	SS
2131−021.....	1.22	7.6×10^{26}	1995 Jul	1.3	1.5	0.7	9	0.83	9.30×10^{9}	SS
2134+004.....	5.51	2.9×10^{28}	1995 Jul	4.3	1.3	0.6	9	2.21	6.30×10^{10}	SS
2136+141.....	1.92	1.4×10^{28}	1995 Jul	2.0	1.2	0.6	14	1.45	5.21×10^{10}	SS
2144+092.....	0.56	1.2×10^{27}	1995 Jul	1.4	1.2	0.6	13	0.44	9.79×10^{9}	SS
2145+067.....	6.52	1.1×10^{28}	1997 Mar	7.9	1.1	0.6	3	3.70	8.45×10^{10}	C
2200+420.....	3.23	3.7×10^{25}	1997 Mar	3.2	1.0	0.6	7	1.49	2.00×10^{10}	SS
2201+315.....	3.10	6.1×10^{26}	1997 Mar	2.4	1.0	0.5	5	2.28	4.48×10^{10}	SS
2209+236.....	0.91	...	1995 Apr	2.3	0.9	0.5	6	0.80	1.35×10^{10}	SS
2223−052.....	3.92	1.2×10^{28}	1997 Mar	2.3	1.2	0.5	5	3.28	9.93×10^{10}	SS
2230+114.....	2.33	4.3×10^{27}	1995 Jul	2.5	1.3	0.7	16	0.81	1.37×10^{10}	SS
2234+282.....	1.21	1.4×10^{27}	1995 Apr	2.1	0.9	0.5	2	0.74	2.25×10^{10}	SS
2243−123.....	2.56	2.0×10^{27}	1997 Mar	1.9	1.2	0.5	0	1.85	3.80×10^{10}	SS
2251+158.....	8.86	1.2×10^{28}	1997 Mar	5.5	1.1	0.6	10	4.24	9.02×10^{10}	SS
2345−167.....	1.60	1.1×10^{27}	1997 Mar	1.8	1.2	0.5	4	0.75	1.50×10^{10}	SS

wavelengths, and, where appropriate, other recently published VLBI observations.

Sources that contain only a single barely resolved component are noted as C or "compact." None of these sources is completely unresolved, but they will nevertheless be useful as calibrators for future VLBA observations at 2 cm or at nearby wavelengths. In some of these sources, examination of the fringe visibility plots show clear evidence of structure that is not apparent in the images restored with the nominal beamwidth. In the notes to individual sources, where appropriate, we give the structure of these barely resolved sources based on model fitting.

The measured peak brightness temperatures for the most compact sources, as derived from fitting Gaussian components to the (u, v) data, are in the range of 10^{11}–10^{12} K. However, only a few sources have an observed brightness temperature that approaches the limit of 10^{12} K normally expected from a stationary source cooled by inverse

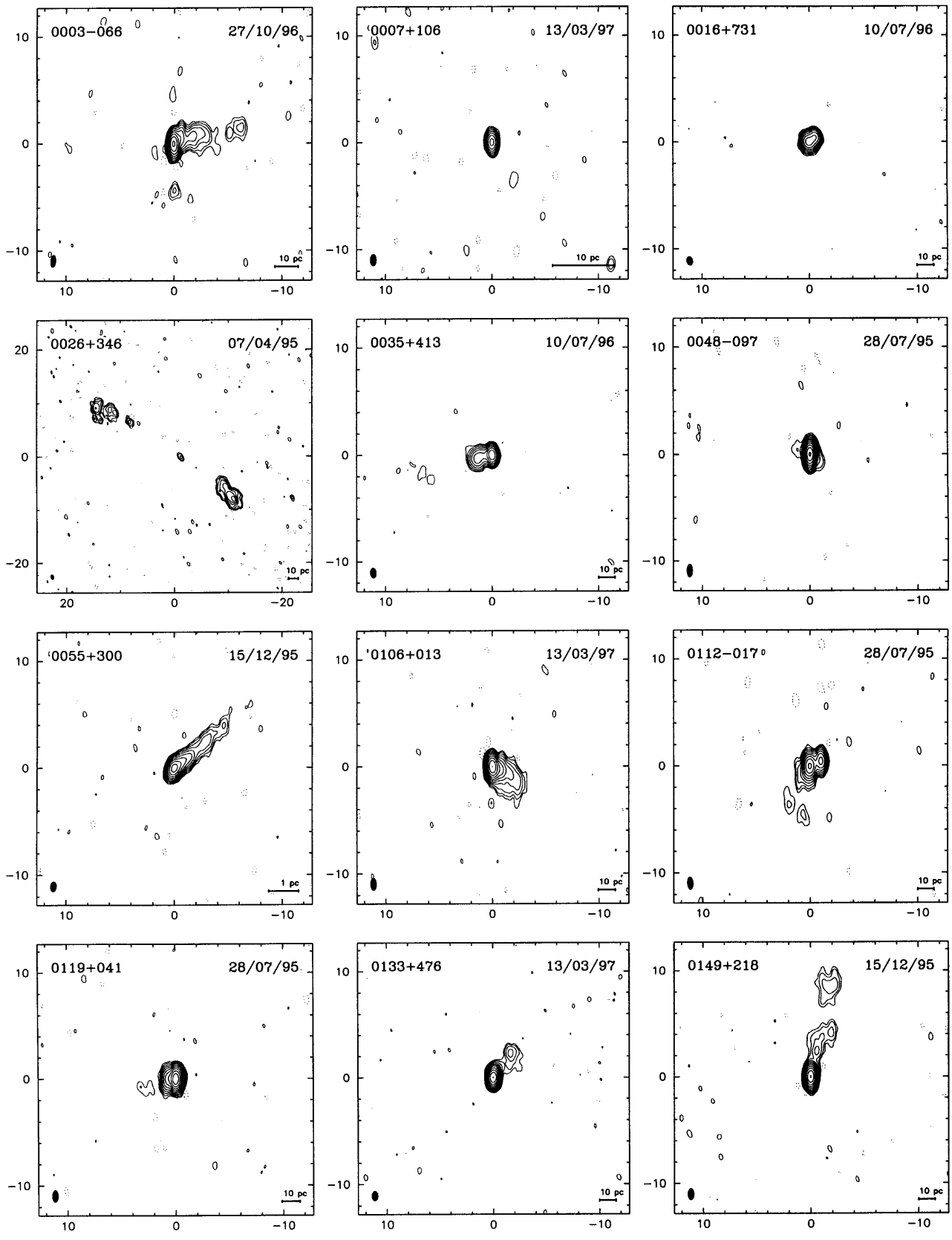

FIG. 2.—Contour maps of our 132 sources. The lowest contour level is at 3 times the rms noise and is listed in col. (5) of Table 3. Other contours are shown at increasing powers of 2. The peak flux density in each image is given in col. (9) of Table 3, and the major axis, minor axis, and position angle of the resorting beam are given in cols. (6)–(8). Most images are centered on the brightest component, but for a few of the larger asymmetric sources, we have shifted the center to fit the image in the 25.6 mas box. Note that while most of the displayed boxes are 25.6 mas on a side, a few of the larger sources are shown in a box twice this size. Each panel also shows a bar representing a linear scale of 10 pc for sources with $z > 0.1$ and 1 pc for sources with $z < 0.1$. The two components of the lensed source 0218+357 are shown in the same panel, with the 335 mas separation largely removed.

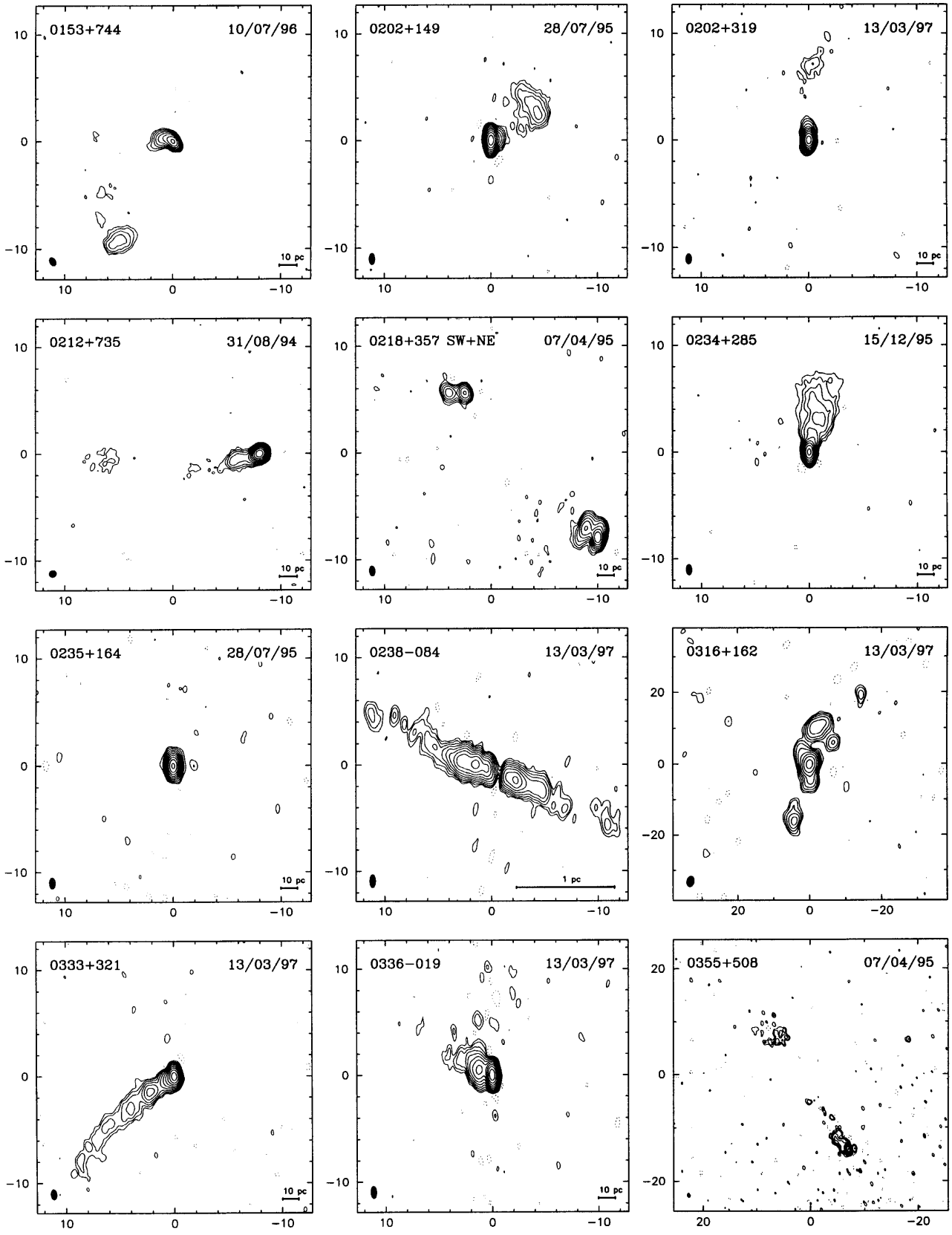

FIG. 2.—*Continued*

Compton radiation. This is perhaps surprising, as it is widely assumed that the most compact feature is the base of a relativistic jet where it turns optically thin (Blandford & Königl 1979) and that Doppler boosting might be expected to increase the observed brightness temperature beyond the inverse Compton limit. We note also that the nominal brightness temperature limit of 10^{12} K is for an idealized homogeneous source with simple geometry (Kellermann &

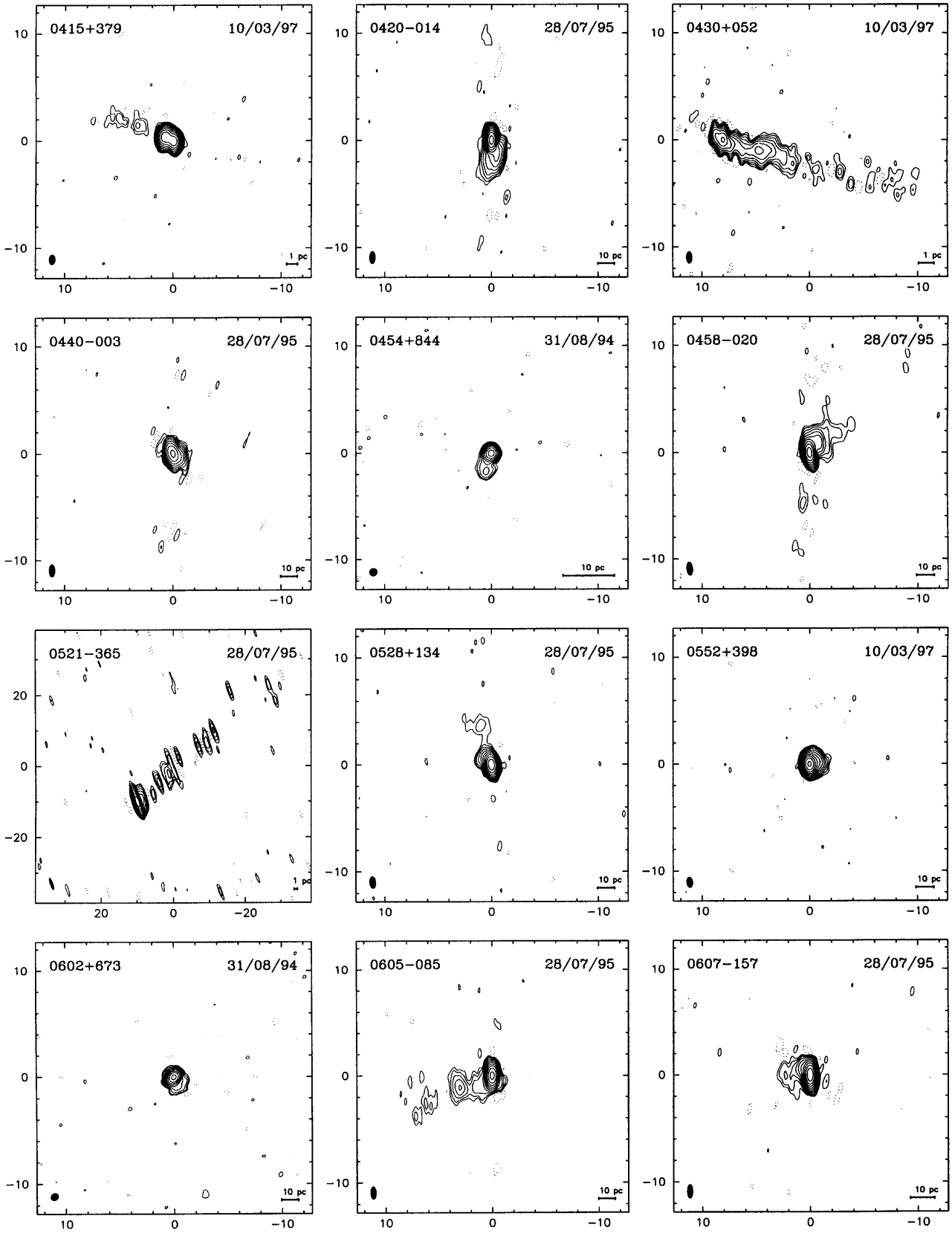

FIG. 2.—*Continued*

Pauliny-Toth 1969), and that higher brightness temperatures might be observed from more complex geometries.

Using an antenna in space with baselines up to 2.15 Earth diameters at 2.3 GHz, Linfield et al. (1989) reported measured brightness temperatures up to 4×10^{12} K, in apparent excess of the inverse Compton limit. Although it is difficult to measure brightness temperatures above 10^{12} K from Earth-sized baselines, self-calibration of our 10-element array gives a robust calibration that is difficult to

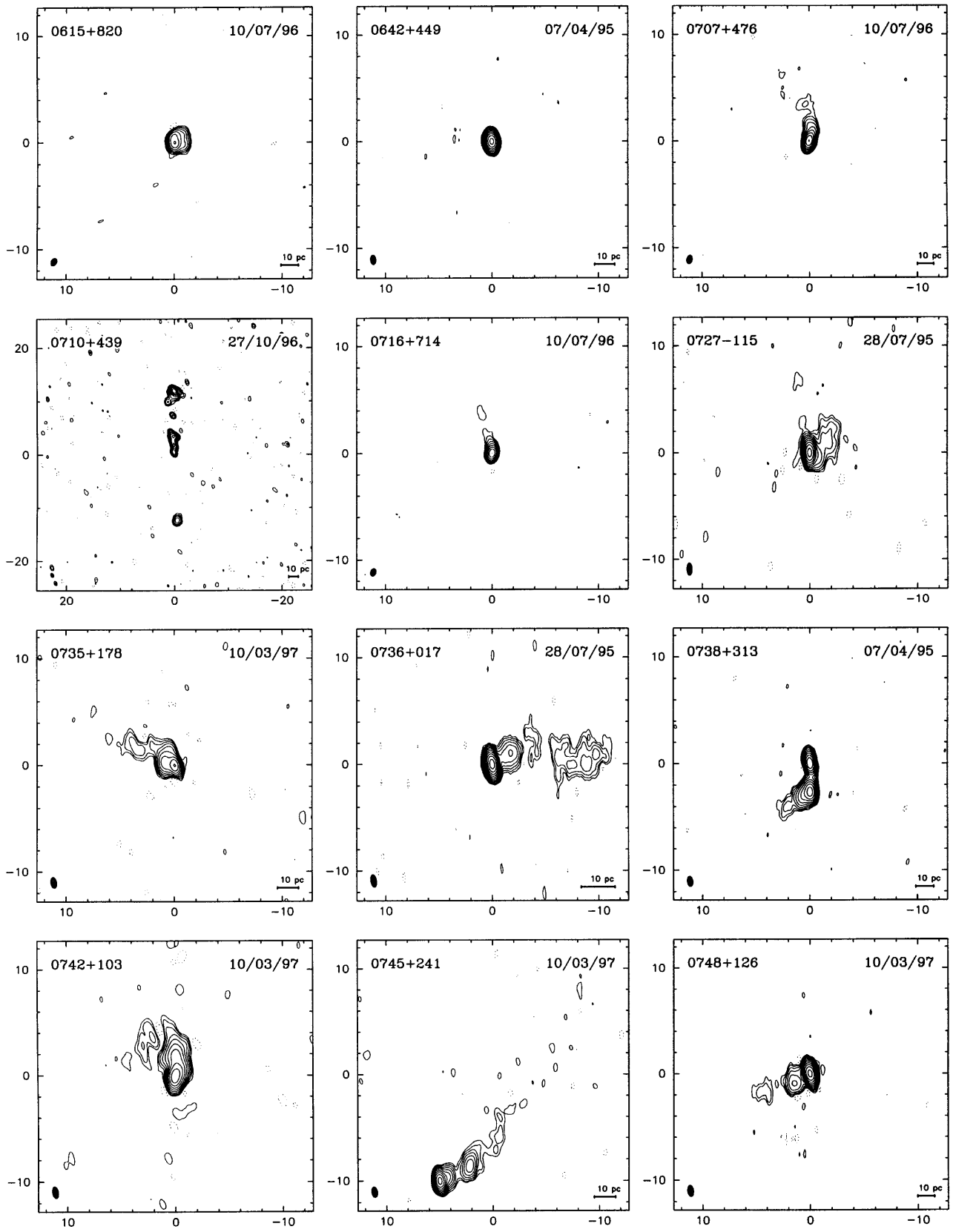

FIG. 2.—*Continued*

obtain from a single distant element, such as from an orbiting antenna. Our sensitivity and calibration are sufficiently good that on our longest baselines, near 400 Mλ, we can determine the fringe visibility to a few percent; so we can, with confidence, say that a source is resolved if the observed fringe visibility is less than 0.9. This corresponds to a diameter of 0.1 mas or, for a 1 Jy source (with $z = 0$), a brightness temperature of 8×10^{11} K. We cannot exclude the possi-

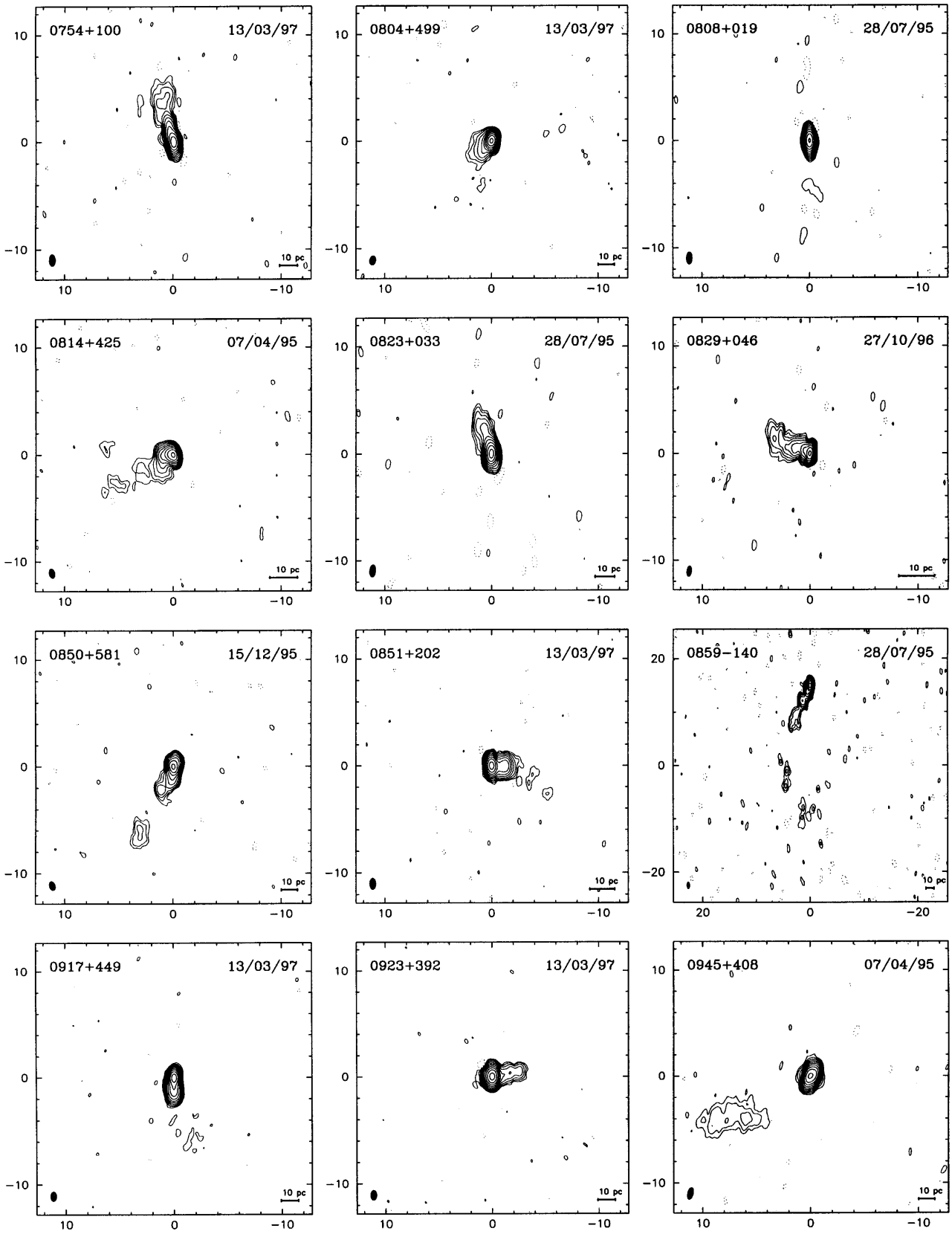

FIG. 2.—*Continued*

bility that some fraction of the observed flux is in an unresolved component embedded in the larger structure, but there is little evidence from examination of our visibility plots for any unresolved structure that might reflect relativistically boosted jets with apparent brightness temperatures in excess of 10^{12} K.

In nearly all of the well-resolved sources, there is a single component with dimensions not exceeding that of the syn-

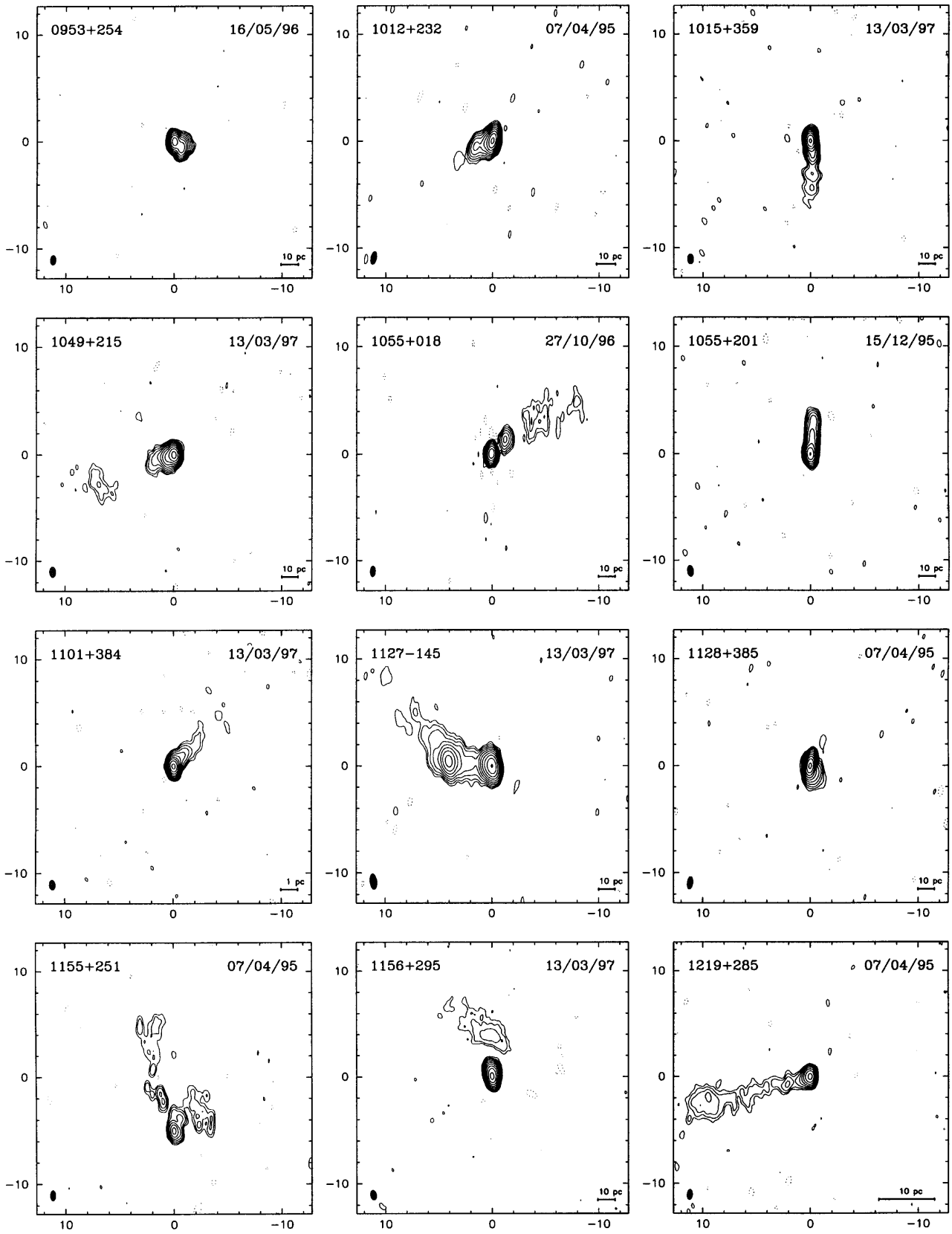

FIG. 2.—*Continued*

thesized beam and generally located near one of the extremities. These asymmetric structures, which we classify as single-sided (SS), are characteristic of the familiar core-jet structure that has been used to describe other milliarcsecond VLBI observations. It is believed that this is the result of differential Doppler boosting of an intrinsic twin-jet structure.

In many of the sources with jetlike structure, the jet bends through angles up to 90° or even more. In some cases, the curvature is gradual, but in other sources the jet shows

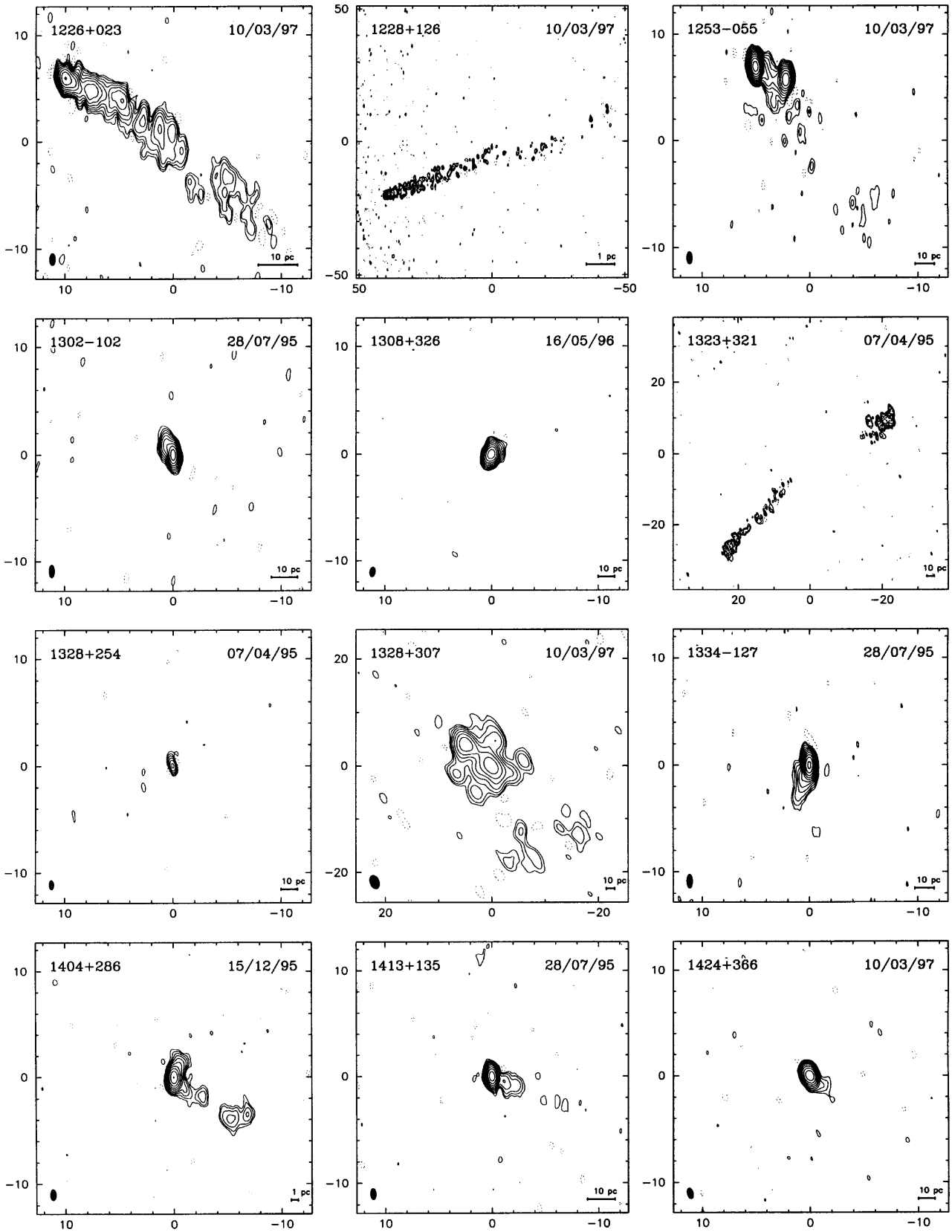

FIG. 2.—*Continued*

remarkably sharp bends or twists, especially close to the core. Generally, the jet appears unresolved in the direction transverse to its extent, but a few sources have broad plumes. In other sources, the jet is seen to wiggle through several turns of a few tens of degrees in alternate directions. While in some sources the jet appears truly continuous, in others the jet appears to contain multiple more or less discrete components. It is not clear whether this represents a

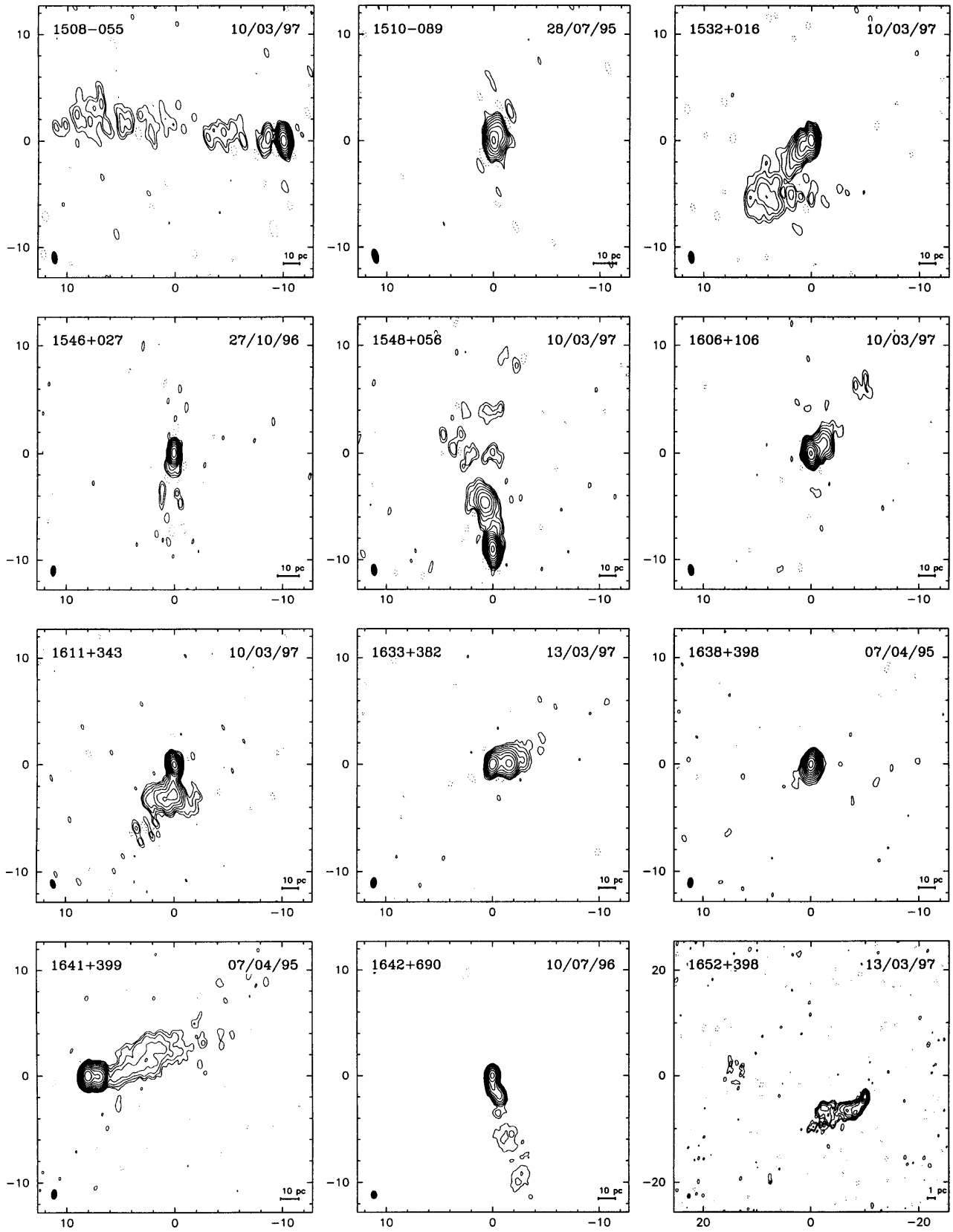

FIG. 2.—*Continued*

real distinction or, rather, a limited dynamic range of the image.

A few sources show more symmetric double structure or contain three or more components, usually with the central one being the most compact. We refer to these sources as double-sided (DS). The nature of the symmetric DS sources is unclear, and it is also not clear whether they form a single category. Possible interpretations include (1) gravitational

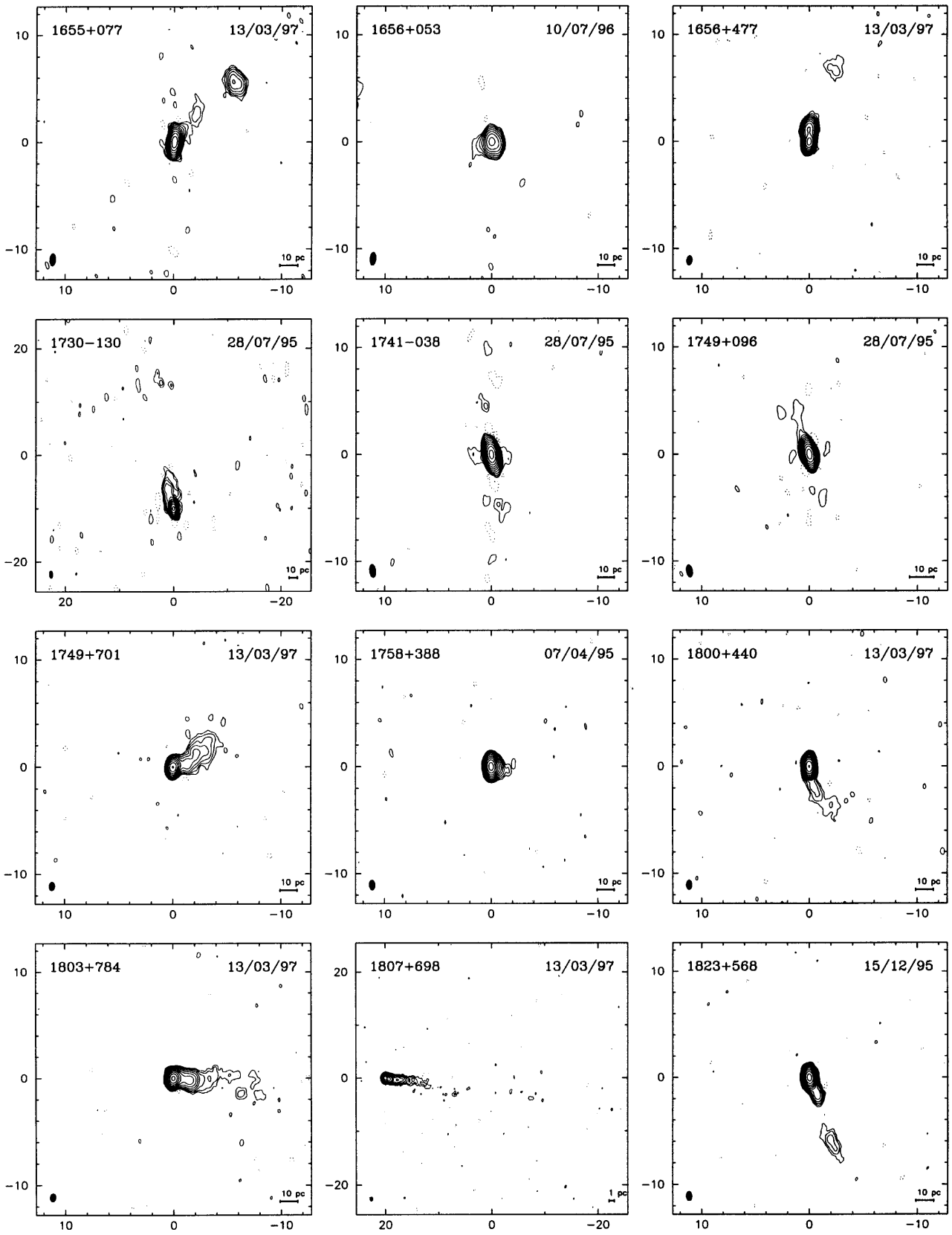

FIG. 2.—*Continued*

minilensing from black holes of the order of $10^6\ M_\odot$ (e.g., Lacey & Ostriker 1985); (2) confined classical doubles (O'Dea, Baum, & Stanghellini 1991); (3) young doubles (Fanti et al. 1995; Readhead et al. 1996a); (4) reborn doubles (Baum et al. 1990); and (5) twin-jet sources in the plane of the sky or that move with subrelativistic velocity. The double-sided appearance may also be due to a single jet that, in projection, appears to wrap around both sides of the

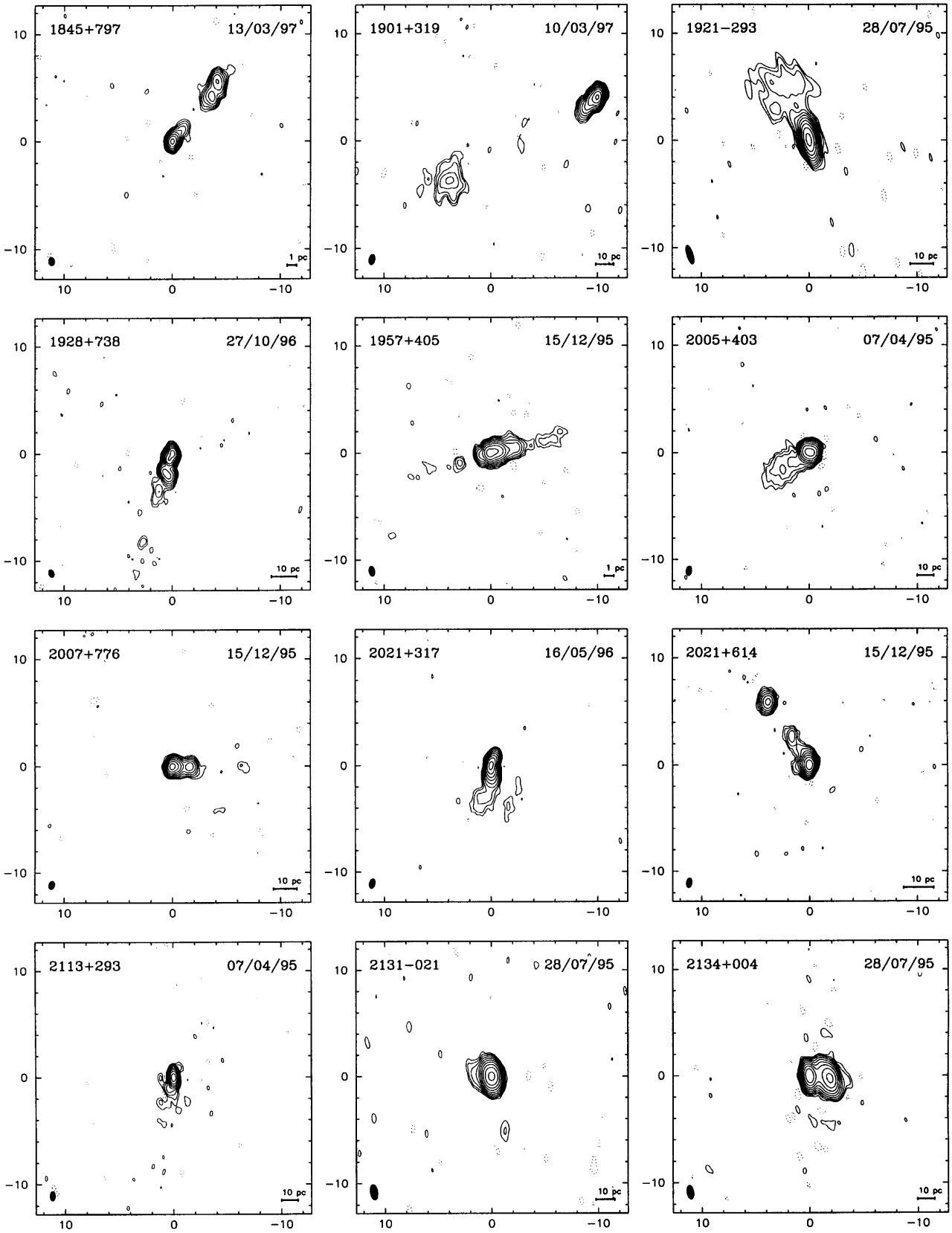

FIG. 2.—*Continued*

nucleus. Because of relativistic boosting, the jet appears bright first on one side as it approaches the viewer, fades as it bends across the nucleus, and then brightens again as it curves around and approaches the viewer again from the other side.

Both NGC 1052 (0238−084; Vermeulen et al. 1998) and Cygnus A (1957+405) show more symmetric structure at 15 GHz than seen at longer wavelengths (cf. Krichbaum et al. 1998; Sorathia et al. 1996). We note that similar phenomena have been reported in other low-luminosity radio galaxies,

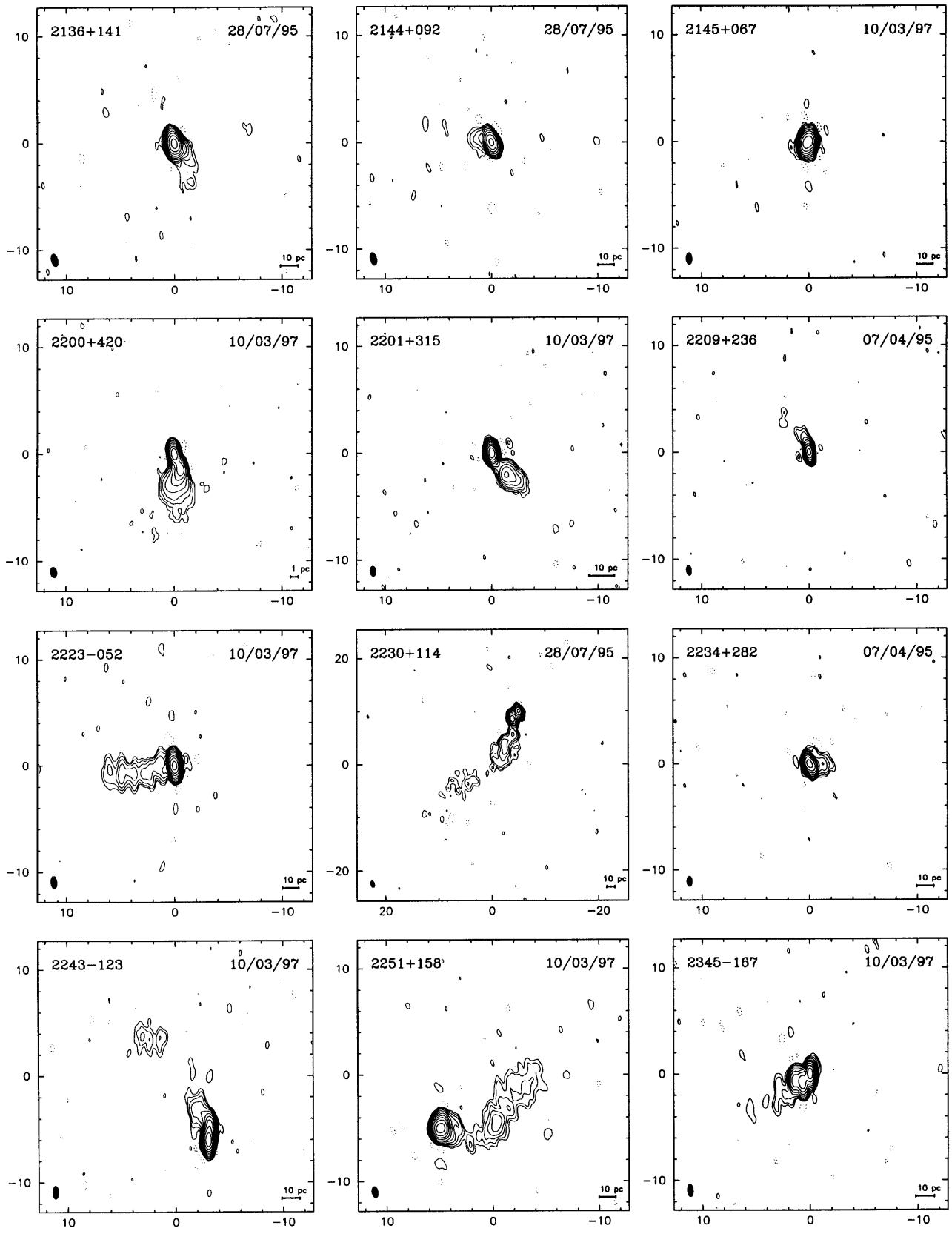

FIG. 2.—*Continued*

such as NGC 1275 (Walker et al. 1998), NGC 4258 (Herrnstein et al. 1997), Hydra A (3C 218; Taylor 1996), NGC 4261 (3C 270; Jones & Wehrle 1997), NGC 5128 (Jones et al. 1996), PKS 1413+135 (Perlman et al. 1996), and Mrk 231 (Ulvestad, Wrobel, & Carilli 1998). These high-frequency, symmetric sources are all identified with galaxies rather than quasars and all have radio luminosities less than 10^{26} W Hz^{-1}. The asymmetry observed on parsec scales at the longer wavelengths in these sources has been interpreted in terms of free-free absorption from a sur-

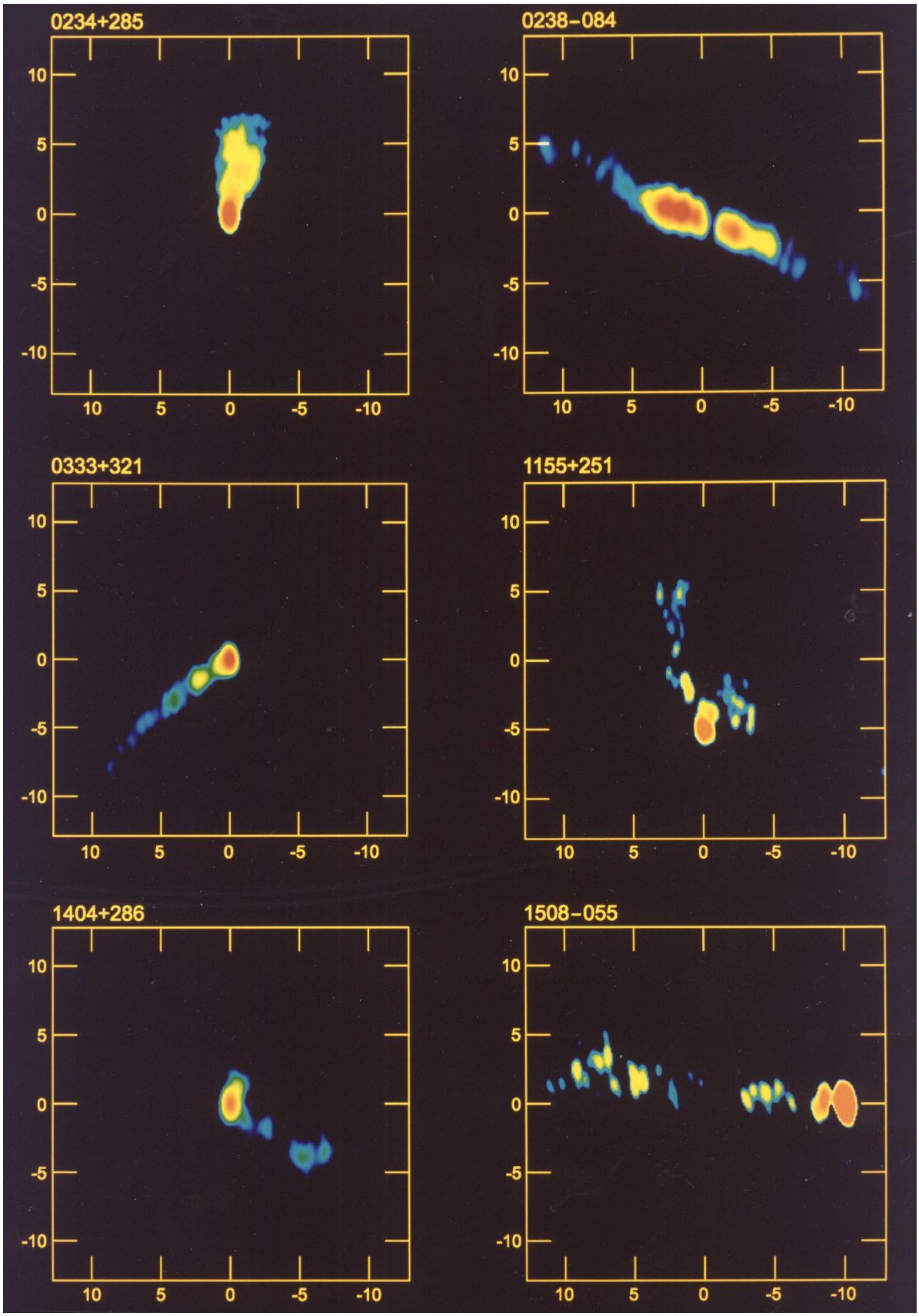

FIG. 3.—Color images of six sources illustrating the range of structures observed. Axes show the offset from the center of the image in milliarcseconds.

rounding torus (e.g., Levinson, Laor, & Vermeulen 1995). The surrounding material, in at least some of these sources, is known from H I absorption, and H_2O and OH maser emission, to also have an atomic and molecular component (see Conway & Blanco 1995 and references above).

The other sources in our sample that we classify as double-sided are 0026+346, 0048−097, 0710+439, 1323+321, 1404+286, and 2021+317. All of these sources, except 0048−097, are included in the (O'Dea et al. 1991) list of gigahertz-peaked spectrum (GPS) sources, which show a sharp low-frequency spectral cutoff near 1 GHz, are identified with galaxies, and have radio luminosity less than about 10^{26} W Hz^{-1}. The data presented by Kühr et al. (1981) indicate that the BL Lac object 0048−097, as well, is a GPS source. The source 0710+439 has been described as a CSO by Taylor, Readhead, & Pearson (1996a), and the other five also appear from our data to have a milliarcsecond morphology characteristic of CSOs. In all of these symmetric or double-sided sources, there is no evidence of the effect of differential Doppler boosting, possibly because the source is oriented close to the plane of the sky, or because the motion is nonrelativistic. However, it is not clear how these powerful CSOs are related to the low-luminosity symmetric radio galaxies discussed above, but they too seem to have a relatively large ambient gas density, as evidenced by recent detections of H I absorption (Vermeulen et al. 1998)

Other sources in our sample that are classified as GPS sources by O'Dea et al. (1991) are 0153+744, 0316+161, 0528+134, 0552+398, 0615+820, 0738+313, and 2230+114. In addition, 2134+004 is a well-known GPS source (Shimmins et al. 1968). Except possibly for the optically faint source 0316+161, which does not have a measured redshift, these GPS sources all have a luminosity at 15 GHz much greater than 10^{26} W Hz^{-1} and are identified with quasars rather than galaxies. Earlier lower resolution observations of many GPS sources have been interpreted in terms of compact double structure (e.g., Phillips & Mutel 1982). However, our observations suggest a more diverse distribution of morphologies, at least for the more luminous GPS sources, which all appear asymmetric except 0316+161, which has an irregular structure.

The GPS sources are characterized by a sharp low-frequency cutoff in their radio spectra, which might be due to either synchrotron self-absorption, free-free absorption in a foreground screen, or the effects of a dispersive medium (see, e.g., Kellermann 1966). Considering the apparent asymmetry seen in our images of the more powerful GPS sources, and the correspondingly wide range of surface brightness, it is difficult to understand the observed sharp spectral cutoffs of these GPS sources in terms of simple self-absorption. Observations of these sources at even shorter wavelengths will be important to see whether they appear more symmetric, as would be expected if the low-frequency cutoff is due to free-free absorption, as is found in some of the sources located in galaxies.

Several sources show a complex two-dimensional structure, which we classify as irregular (Irr). Some of these Irr sources, such as 1155+251 and 1611+343, may contain a twisted jet from which we see the relativistically boosted flux from just those regions where the jet is oriented along the line of sight toward the observer. However, we caution that the apparent irregular structure that we observe may simply be the result of inadequate dynamic range and resolution. In particular, our images of these complex sources may be limited by the absence of short spacings in the VLBA.

5. NOTES ON INDIVIDUAL SOURCES

0003−066.—The component about 5 mas to the south is probably an artifact caused by the proximity to the equator.

0007+106.—There is a probable jet that connects the very compact and highly variable core to a 1 mJy component about 15 mas to the southwest. There may also be a weak component roughly the same distance to the northeast.

0016+731.—Model fitting to this compact source indicates a double component structure with a separation of 0.7 mas in P.A. −51 and component flux densities of 0.48 and 0.22 Jy.

0026+346.—We have classified this GPS source as DS assuming that one of the weaker intermediate components is the core of a CSO, but we cannot exclude the possibility that the core is located at one of the extremities.

0048−097.—This source appears to contain very compact double-sided structure.

0153+744.—The faint components seen to the southeast of the brightest component correspond to peaks in a highly curved jet seen by Hummel et al. (1997) at 3.6 and 6 cm.

0202+149.—The jet shows a nearly right-angle bend.

0218+357.—This is by far the closest-spacing lensed image, with a component separation of 335 mas (Patnaik, Porcas, & Browne 1995). We do not give a classification for the structure of this source in Table 3, as the appearance is distorted by the lensing.

0234+285.—There is a very diffuse secondary component.

0238−084.—This bright elliptical galaxy, NGC 1052, has two jets, each containing multiple components moving away from the AGN in opposite directions. The central core is not visible in our 2 cm image. Diamond et al. (1998) report two H_2O maser complexes located in the inner part of the western jet.

0316+162.—CTA 21 is a prototypical GPS source (Kellermann et al. 1962) and has a complex structure.

0336−019.—The faint structure to the north may be artifacts.

0415+379.—While 3C 111 appears clearly one-sided at 2 cm, higher resolution 7 mm observations indicate that the apparent double structure seen at the west end of the 2 cm jet breaks up into a more complex multicomponent symmetric configuration with no obvious component that can be identified as the core (Alef et al. 1998). Our multiepoch 2 cm observations suggest motion toward the east.

0430+052.—This is a well-known superluminal source (3C 120) with a long, thin jet with small oscillations. Observations at 18 cm trace the jet out to 200 mas (Benson et al. 1988).

0458−020.—The jet appears to have a sharp bend within 1 mas of the core. Structure to the south is probably not real.

0528+134.—This is one of the brightest gamma-ray sources detected by EGRET (Mattox et al. 1997) that has been extensively studied at a number of wavelengths (e.g., Krichbaum et al. 1995).

0552+398.—Model fitting of this strong compact source indicates a single-sided structure with 3.9 Jy in a small core and 1.1 Jy in a jet component.

0605−085.—Structure to the west of the brightest component (the core?) could be part of an initial tight loop of a strongly bent jet that continues to the east.

0615+820.—This source does not have a simple linear morphology.

0642+449.—The component seen at 6 cm about 3 mas to the east by Xu et al. (1995) is only marginally detected in our 2 cm observations.

0710+439.—This is a well-known CSO (Taylor et al. 1996a).

0716+714.—This intraday variable has been observed to show intensity changes up to 10% within a day (Wagner et al. 1996).

0727−115.—The jet appears to have a 90° or larger bend.

0735+178.—The jet has multiple sharp curves.

0738+313.—The jet has a well-defined sharp bend with a prominent knot located at the bend.

0742+103.—This GPS QSO is unusually faint at optical and IR wavelengths and is among the class of optically quiet quasars (Stickel et al. 1996). Longer wavelength images (Fey & Charlot 1997) show that the structure seen to the northeast in our 2 cm image is the beginning of a highly bent jet.

0814+425.—The jet that emerges to the east bends sharply to the south. The weak feature seen about 6 mas to the southeast may be part of the structure reported by Aaron (1996) at 18 cm.

0859−140.—A long, thin, curved jet emerges from the core.

0923+392.—The observed structure at 2 cm appears deceptively simple compared with shorter wavelength observations, which show that the western component contains a self-absorbed core (Alberdi et al. 1997). Long-term monitoring of this source shows that there are both stationary and moving components (Alberdi et al. 1993).

0945+408.—There is a very diffuse detached secondary component. The inner bright feature has double structure, which becomes more noticeable in our observations made the following year.

1101+384.—Mrk 421 is the closest known BL Lac object. It is one of the brightest gamma-ray sources in the sky, which has also had a strong TeV flare in 1994 May (Macomb 1995) and again in 1996 May (Zweerink et al. 1997).

1127−145.—There is a prominent knot at the position of a sharp bend.

1155+251.—This is an unusually complex source. The jet direction is unclear, and there is some indication that the northeastern feature splits into two narrow jets.

1219+285.—A long, thin jet terminates in a prominent extended component.

1226+023.—The well-known jet in 3C 273 continues out to a much farther distance (Davis, Unwin, & Muxlow 1991) than shown in our image, which is sensitive only to the higher surface brightness structure.

1228+126.—M87 contains a well-known radio jet (e.g., Biretta & Junor 1995). Our observations show that the inner part is well collimated with sharp edges and has an apparent kink about 45 mas from the core.

1253−055.—The two bright components in 3C 279 are separating along a direction that differs from the direction defined by the lower surface brightness features (see Carrara et al. 1993 for more details).

1323+321.—There is no obvious core in this source, which is suggestive of a CSO morphology.

1328+254.—This source (3C 287) is largely resolved by our observations, which show only a weak compact feature. We do not attempt to classify this structure.

1328+307.—The bright structure seen in our image of 3C 286 is the end of a low surface brightness feature that extends nearly 100 mas to the southwest (Cotton et al. 1997). Cotton et al. suggest that 3C 286 is a normal core-jet source in which the relativistic core (base of the jet) is aimed away from us so that we do not see it, but the jet curves into our line of sight. Thus we see a "naked jet."

1404+286.—From global observations at 6 cm, OQ 208 has been described by Stanghellini et al. (1997) and others as a compact double, characteristic of GPS sources. Our higher resolution observations at 2 cm, however, show a weak core located between two larger, more complex components, suggesting that this source is a CSO. Comparison with the Stanghellini 6 cm image suggests that the central component has an inverted spectrum.

1413+135.—Multiwavelength observations by Perlman et al. (1996) show complex two-sided structure in this source. Our high-resolution 2 cm observations, which are insensitive to the low surface brightness steep-spectrum northeastern jet, show the southwestern jet in more detail than seen at the longer wavelengths. This is an unusually red quasar that is optically quiet (Rieke, Lebovsky, & Kinman 1979; Stickel et al. 1996).

1532+016.—The complex structure nearly due south of the core is probably real and suggestive of a twisted jet.

1611+343.—The complex structure probably reflects a highly twisted jet, which, in projection, loops back across itself.

1641+399.—About 3 mas from the core, the 3C 345 jet has a sharp transition to a diffuse jet that is considerably more prominent at longer wavelengths (Lobanov & Zensus 1998).

1642+690.—The structure and evolution of this source have been described by Venturi et al. (1997) from observations at 3.6 and 6 cm made with lower resolution.

1652+398.—Mrk 501 has a diffuse twisting jet, which has been studied in more detail by Conway & Wrobel (1995). A very high energy ($E > 300$ GeV) gamma-ray flare was observed in 1997 April (Catanese et al. 1997).

1741−038.—The weak components may be artifacts.

1845+797.—An unpublished 6 cm image obtained in 1996 by R. C. V. shows that the northwestern emission has brightened considerably with respect to the 1982 6 cm image shown by Pearson & Readhead (1988). It is likely that the other, southeastern side, which is the most compact and has the flattest spectrum, is the location of the core.

1921−293.—This is one of the strongest sources in the sky at millimeter wavelengths and has an unusually flat spectrum between 1 mm and 1 m. At shorter wavelengths, the spectrum steepens and continues with a spectral index $\alpha \sim -1$ out to at least ultraviolet wavelengths (Shen et al. 1998a). The secondary feature is unusually diffuse. VLBA observations made at 7 mm in 1994 and in 1996 (Shen, Moran, & Kellermann 1998b) show that the jet curves sharply and is elongated along a position angle near −23° out to a distance of about 1 mas (4 pc), where there is an extension in the 7 mm image toward the diffuse jet that we see at 2 cm located about 6 mas away. Observations at 6 cm made in 1996 are consistent with the 7 mm and 2 cm

observations, but 6 cm observations made in 1992 by Shen et al. (1998a) show a secondary feature that lies to the northwest rather than the northeast of the core. Curiously, there is no reported gamma-ray emission from this, one of the brightest known blazars (Mattox et al. 1997).

1957+405.—The double-lobe radio galaxy Cygnus A is one of the most luminous radio galaxies known. At 2 cm, the nucleus contains less than 1% of the total luminosity. The two-sided structure seen in our VLBA image is shown more clearly in the images of Sorathia et al. (1996) and Krichbaum et al. (1998) at 0.7, 1.3, and 6 cm.

2021+614.—This GPS source has been suggested as a likely CSO (Henstock & Taylor 1997, private communication).

2131−021.—This object contains a closely spaced double.

2134+004.—We do not see any evidence for the widely discrepant structures previously reported for this source (Pauliny-Toth et al. 1987, 1989). Much of the reported variation may have been the result of inadequate sampling of the (u, v)-plane and due to the proximity of this source to the equator.

2145+067.—Model fitting indicates a double source with a component separation of 0.5 mas in P.A. $-61°$ and flux densities of 3.9 and 2.5 Jy.

2200+420.—The structure of the relatively diffuse jet in BL Lac has been studied in detail by Denn & Mutel (1998).

2230+114.—CTA 102 is a classical GPS source (Kellermann et al. 1962) containing a jet with multiple twists.

2251+158.—The jet in 3C 454.3 has pronounced curvature, which is also seen in 6 cm observations made between 1981 and 1991 (Pauliny-Toth et al. 1987; Pauliny-Toth 1998).

6. GAMMA-RAY EMISSION

Observations with the EGRET telescope aboard the *Compton Gamma Ray Observatory* have shown that strong gamma-ray sources are mostly identified with compact flat-spectrum radio sources, particularly those associated with "blazars" and superluminal sources (e.g., Thompson et al. 1993; von Montigny et al. 1995a; Mattox et al. 1997). This is, perhaps, not surprising, as the gamma-ray emission, like the parsec-scale radio emission, is thought to originate in a highly relativistic jet (see, e.g., Dondi & Ghisellini 1995). However, it is not clear why some compact superluminal radio sources are gamma-ray sources and others are not or, more generally, how gamma-ray compact radio sources differ from the non–gamma-ray compact radio sources. Curiously, gamma-ray emission has not been detected from some of the most prominent superluminal blazars, such as 3C 120 and 3C 345, or from the bright millimeter blazar 1921−293. While the detailed mechanism for the production of gamma radiation is unclear, it probably takes place close to the central engine (see, e.g., von Montigny et al. 1995a) or at the base of the relativistic jet (Mattox et al. 1997). Our radio observations probe close to the central engine, but farther out than the likely source of gamma-ray emission. Still we might expect to find differences in the sub-milliarcsecond radio morphology between gamma-ray and non–gamma-ray sources, especially if, like the radio emission, the gamma-ray emission is beamed and the observed flux density is orientation dependent.

While there may be intrinsic differences among quasars and AGNs in their gamma-ray–to–radio luminosity ratio, the high apparent gamma-ray luminosity, combined with the observed rapid variability, suggests that the gamma-ray emission, like the radio emission, must be beamed. Consideration of relativistic beaming models suggests that there might be a correlation between observed gamma-ray luminosity and the radio morphology, both of which reflect the source orientation. In particular, if the gamma-ray emission is more highly beamed than the radio, then gamma-ray sources would be, on average, viewed more closely aligned to the line of sight, and this would be reflected in the observed sub-milliarcsecond radio morphology.

Gamma-ray emission has been observed above 100 MeV energy with EGRET for 26 of the sources listed in Table 1 (Mattox et al. 1997). Twenty-three other sources in our sample were observed with EGRET but had no detectable gamma-ray emission (von Montigny et al. 1995b). We find no obvious difference in the radio morphology between these two groups, contrary to what might be expected if the gamma-ray emission is beamed in a more narrow cone than the radio emission, or if there is otherwise a close coupling between the radio and gamma-ray emission.

The absence of any apparent correlation between observed gamma-ray emission and compact structure is perhaps not surprising. Although gamma-ray sources are often identified with bright compact radio sources, the range of gamma-ray fluxes seen by EGRET is only about a factor of 100, and most sources lie within a factor of 10 of the minimum detectable flux. Nearly all EGRET sources are detected only at the time of a strong flare (Mattox et al. 1997). Therefore, it is not unlikely that the other sources in our sample are also gamma-ray emitters, but are somewhat below the detection level of EGRET or flared at a time when not observed by EGRET. While it will be of interest to obtain complete high-resolution radio images for the remaining sources detected by EGRET and to compare their dynamics with those of the nondetections, we do not expect that concentration on the few sources that happened to be above the EGRET detection limit at the time of observation will be of any special interest.

These observations have depended on the support of many individuals at the NRAO and at Caltech. Our automated DIFMAP procedure was based on scripts written by Martin Shepherd and Greg Taylor. Craig Walker provided up-to-date gain curves for each VLBA antenna, as well as the scheduling program. Jon Romney, Peggy Perley, and others arranged for the correlation of the data and established the validity of the correlator output. Bill Cotton, Phil Diamond, Eric Greison, Athol Kemball, Leonid Kogan, Pat Murphy, and others gave generously of their time to help us through a multitude of problems with implementing new features of the AIPS software package. John Armstrong, a Research Experience for Undergraduates student, participated in some of the data reduction in the summer of 1996. We are grateful to all of them for their conscientious support. We also thank the referee, Tim Pearson, for his careful reading of the manuscript and his many constructive suggestions, which have helped to improve the paper. R. C. V. was supported in part by NSF grants AST 91-17100 and AST 94-20018, and M. H. C. by NSF grant AST 91-21889. This research has

made use of the NASA/IPAC Extragalactic Database (NED), which is operated by the Jet Propulsion Laboratory, Caltech, under contract with the National Aeronautics and Space Administration.

REFERENCES

Aaron, S. 1996, Ph.D. thesis, Brandeis Univ.
Alberdi, A., et al. 1997, A&A, 327, 513
———. 1993, A&A, 271, 93
Alef, W., Preuss, E., Kellermann, K. I., & Gabuzda, D. 1998, in IAU Colloq. 164, Radio Emission from Galactic and Extragalactic Compact Sources, ed. J. A. Zensus, J. M. Wrobel, & G. B. Taylor (San Francisco: ASP), in press
Baum, S. A., O'Dea, C. P., Murphy, D. W., & de Bruyn, A. G. 1990, A&A, 232, 19
Benson, J. M., Walker, R. C., Unwin, S. C., Muxlow, T. W. B., Wilkinson, P. N., Booth, R. S., Pilbratt, G., & Simon, R. S. 1988, ApJ, 334, 560
Biretta, J. A., & Junor, W. 1995, Proc. Natl. Acad. Sci., 92, 11364
Blandford, R. D., & Königl, A. 1979, ApJ, 232, 34
Blandford, R. D., & Rees, M. 1974, MNRAS, 169, 395
Bridle, A. H., & Perley, R. A. 1984, ARA&A, 22, 319
Carrara, E. A., Abraham, Z., Unwin, S. C., & Zensus, J. A. 1993, A&A, 279, 83
Catanese, M., et al. 1997, ApJ, 487, L143
Conway, J. E., & Blanco, P. R. 1995, ApJ, 449, L131
Conway, J. E., & Wrobel, J. M. 1995, ApJ 439, 98
Cotton, W. D., Fanti, C., Fanti, R., Dallacasa, D., Foley, A. R., Schilizzi, R. T., & Spencer, R. E. 1997, A&A, 325, 479
Davis, R. J., Unwin, S. C., & Muxlow, T. W. B. 1991, Nature, 354, 374
Denn, G. R., & Mutel, R. L. 1998, in IAU Colloq. 164, Radio Emission from Galactic and Extragalactic Compact Sources, ed. J. A. Zensus, J. M. Wrobel, & G. B. Taylor (San Francisco: ASP), in press
Diamond, P. J., Claussen, M. J., Braatz, J. A., Wilson, A. S., & Henkel, C. 1998, in IAU Colloq. 164, Radio Emission from Galactic and Extragalactic Compact Sources, ed. J. A. Zensus, J. M. Wrobel, & G. B. Taylor (San Francisco: ASP), in press
Dondi, L., & Ghisellini, G. 1995, MNRAS, 273, 583
Fanti, C., Fanti, R., Dallacasa, D., Schilizzi, R. T., Spencer, R. E., & Stanghellini, C. 1995, A&A, 302, 317
Fey, A. L., & Charlot, P. 1997, ApJS, 111, 95
Fey, A. L., Clegg, A. W., & Fomalont, E. 1996, ApJS, 105, 299
Henstock, D. R., Browne, I. W. A., Wilkinson, P. N., Taylor, G. B., Vermeulen, R. C., Pearson, T. J., & Readhead, A. C. S. 1995, ApJS, 100, 1
Herbig, T., & Readhead, A. C. S. 1995, ApJS, 81, 83
Herrnstein, J. R., Moran, J. M., Greenhill, L. J., Diamond, P. J., Miyoshi, M., Nakai, N., & Inoue, M. 1997, ApJ, 475, L17
Hummel, C. A., Krichbaum, T. P., Witzel, A., Wullner, K. H., Steffen, W., Alef, W., & Fey, A. 1997, A&A, 324, 857
Jones, D. L., et al. 1996, ApJ, 446, L63
Jones, D. L., & Wehrle, A. E. 1997, ApJ, 484, 186
Kellermann, K. I. 1966, Australian J. Phys., 19, 195
Kellermann, K. I., Long, R. J., Allen, L. R., & Moran, J. M. 1962, Nature, 195, 69
Kellermann, K. I., & Pauliny-Toth, I. I. K. 1969, ApJ, 155, L71
Krichbaum, T. P., Alef, W., Witzel, A., Zensus, J. A., Booth, R. S., Greve, A., & Rogers, A. E. E. 1998, A&A, 329, 873
Krichbaum, T. P., Britzen, S., Standke, K. J., Witzel, A., Schalinski, C. J., & Zensus, J. A. 1995, Proc. Natl. Acad. Sci., 92, 11377
Kühr, H., Witzel, A., Pauliny-Toth, I. I. K., & Nauber, U. 1981, A&AS, 45, 367
Lacey, C. G., & Ostriker, J. P. 1985, ApJ 299, 633
Levinson, A., Laor, A., & Vermeulen, R. C. 1995, ApJ, 448, 589
Linfield, R. P., et al. 1989, ApJ, 336, 1105
Lobanov, A. P., & Zensus, J. A. 1998, ApJ, submitted
Macomb, D. J. 1995, ApJ, 449, L99
Mattox, J. R., Schachter, J., Molnar, L., Hartman, R. C., & Patnaik, A. R. 1997, ApJ, 481, 95
Napier, P. J., Bagri, D. S., Clark, B. G., Rogers, A. E. E., & Romney, J. D. 1994, Proc. IEEE, 82, 658
O'Dea, C. P., Baum, S. A., & Stanghellini, C. 1991, ApJ, 380, 66
Patnaik, A. R., Porcas, R. W., & Browne, I. W. A. 1995, MNRAS, 274, L5
Pauliny-Toth, I. I. K. 1998, in IAU Colloq. 164, Radio Emission from Galactic and Extragalactic Compact Sources, ed. J. A. Zensus, J. M. Wrobel, & G. B. Taylor (San Francisco: ASP), in press
Pauliny-Toth, I. I. K., Porcas, R. W., Zensus, J. A., Kellermann, K. I., Wu, S. Y., Nicholson, G. D., & Mantovani, F. 1987, Nature, 328, 778
Pauliny-Toth, I. I. K., Zensus, J. A., Cohen, M. H., Alberdi, A., & Schaal, R. 1989, in Parsec-Scale Radio Jets, ed. J. A. Zensus & T. J. Pearson (Cambridge: Cambridge Univ. Press), 55
Pearson, T. J., & Readhead, A. C. S. 1981, ApJ, 248, 61
———. 1988, ApJ, 328, 114
Peck, A., & Beasley, A. 1998, in IAU Colloq. 164, Radio Emission from Galactic and Extragalactic Compact Sources, ed. J. A. Zensus, J. M. Wrobel, & G. B. Taylor (San Francisco: ASP), in press
Perlman, E. S., Carilli, C. L., Stocke, J., T., & Conway, J. 1996, AJ, 111, 1839
Phillips, R. B., & Mutel, R. L. 1982, A&A, 106, 21
Polatidis, A. G., Wilkinson, P. N., Xu, W., Readhead, A. C. S., Pearson, T. J., Taylor, G. B., & Vermeulen, R. C. 1995, ApJS, 98, 1
Readhead, A. C. S., Taylor, G. B., Pearson, T. J., & Wilkinson, P. N. 1996a, ApJ, 460, 634
Readhead, A. C. S., Taylor, G. B., Xu, W., Pearson, T. J., Wilkinson, P. N., & Polatidis, A. G. 1996b, ApJ, 460, 612
Rieke, G. H., Lebovsky, M. J., & Kinman, T. D. 1979, ApJ, 232, L151
Shen, E., et al. 1998a, AJ, 115, 1357
Shen, Z.-Q., Moran, J. M., & Kellermann, K. I. 1998b, in preparation
Shepherd, M. C., Pearson, T. J., & Taylor, G. B. 1994a, BAAS, 26, 987
———. 1994b, BAAS, 26, 1318
Shimmins, A. J., Searle, L., Andrew, B. H., & Brandie, G. W. 1968, Astrophys. Lett., 1, 167
Sorathia, B., Bartel, N., Bietenholtz, M., Carilli, C., & Diamond, P. 1996, in Cygnus A: Study of a Radio Galaxy, ed. C. L. Carilli & D. E. Harris (Cambridge: Cambridge Univ. Press), 86
Stanghellini, C., Bondi, M., Dallacasa, D., O'Dea, C. P., Baum, S. A., Fanti, R., & Fanti, C. 1997, A&A, 318, 376
Stickel, M., Meisenheimer, K., & Kühr, H. 1994, A&AS, 105, 211
Stickel, M., Rieke, G. H., Kühr, H., & Rieke, M. J. 1996, ApJ, 468, 556
Taylor, G. B. 1996, ApJ, 470, 394
Taylor, G. B., Readhead, A. C. S., & Pearson, T. J. 1996a, ApJ, 463, 95
Taylor, G. B., Vermeulen, R. C., Pearson, T. J., Readhead, A. C. S., Henstock, D. R., Browne, I. W. A., & Wilkinson, P. N. 1994, ApJS, 95, 345
Taylor, G. B., Vermeulen, R. C., Readhead, A. C. S., Pearson, T. J., Henstock, D. R., & Wilkinson, P. N. 1996b, ApJS, 107, 37
Thakkar, D. D., Xu, W., Readhead, A. C. S., Pearson, T. J., Taylor, G. B., Vermeulen, R. C., Polatidis, A. G., & Wilkinson, P. N. 1995, ApJS, 98, 33
Thompson, D. J., et al. 1993, ApJ, 410, 87
Ulvestad, J. S., Wrobel, J. M., & Carilli, C. L. 1998, in IAU Colloq. 164, Radio Emission from Galactic and Extragalactic Compact Sources, ed. J. A. Zensus, J. M. Wrobel, & G. B. Taylor (San Francisco: ASP), in press
Venturi, T., Pearson, T. J., Barthel, P. D., & Unwin, S. C. 1997, A&A, 325, 484
Vermeulen, R., & Cohen, M. H. 1994, ApJ, 430, 467
von Montigny, C., et al. 1995a, ApJ, 440, 525
———. 1995b, A&A, 299, 680
Wagner, S. J., et al. 1996, AJ, 111, 2187
Walker, R. C., Kellermann, K. I., Dhawan, V., Romney, J. D., Benson, J. M., Vermeulen, R. C., & Alef, W. 1998, in IAU Colloq. 164, Radio Emission from Galactic and Extragalactic Compact Sources, ed. J. A. Zensus, J. M. Wrobel, & G. B. Taylor (San Francisco: ASP), in press
Wilkinson, P. N. 1995, Proc. Natl. Acad. Sci., 92, 11342
Wilkinson, P. N., Polatidis, A. G., Readhead, A. C. S., Xu, W., & Pearson, T. J. 1994, ApJ, 432, L87
Xu, W., Readhead, A. C. S., Pearson, T. J., Polatidis, A. G., & Wilkinson, P. N. 1995, ApJS, 99, 297
Zensus, J. A. 1997, ARA&A, 35, 607
Zweerink, J. A., et al. 1997, ApJ, 490, L141